MIT Joint Program on the Science and Policy of Global Change

Methane Fluxes Between Terrestrial Ecosystems and the Atmosphere at Northern High Latitudes During the Past Century: *A Retrospective Analysis with a Process-Based Biogeochemistry Model*

Qianlai Zhuang, Jerry M. Melillo, David W. Kicklighter, Ronald G. Prinn, A. David McGuire, Paul A. Steudler, Benjamin S. Felzer and Shaomin Hu

Report No. 108
March 2004

The MIT Joint Program on the Science and Policy of Global Change is an organization for research, independent policy analysis, and public education in global environmental change. It seeks to provide leadership in understanding scientific, economic, and ecological aspects of this difficult issue, and combining them into policy assessments that serve the needs of ongoing national and international discussions. To this end, the Program brings together an interdisciplinary group from two established research centers at MIT: the Center for Global Change Science (CGCS) and the Center for Energy and Environmental Policy Research (CEEPR). These two centers bridge many key areas of the needed intellectual work, and additional essential areas are covered by other MIT departments, by collaboration with the Ecosystems Center of the Marine Biology Laboratory (MBL) at Woods Hole, and by short- and long-term visitors to the Program. The Program involves sponsorship and active participation by industry, government, and non-profit organizations.

To inform processes of policy development and implementation, climate change research needs to focus on improving the prediction of those variables that are most relevant to economic, social, and environmental effects. In turn, the greenhouse gas and atmospheric aerosol assumptions underlying climate analysis need to be related to the economic, technological, and political forces that drive emissions, and to the results of international agreements and mitigation. Further, assessments of possible societal and ecosystem impacts, and analysis of mitigation strategies, need to be based on realistic evaluation of the uncertainties of climate science.

This report is one of a series intended to communicate research results and improve public understanding of climate issues, thereby contributing to informed debate about the climate issue, the uncertainties, and the economic and social implications of policy alternatives. Titles in the Report Series to date are listed on the inside back cover.

Henry D. Jacoby and Ronald G. Prinn,
Program Co-Directors

For more information, please contact the Joint Program Office

Postal Address: Joint Program on the Science and Policy of Global Change
77 Massachusetts Avenue
MIT E40-428
Cambridge MA 02139-4307 (USA)

Location: One Amherst Street, Cambridge
Building E40, Room 428
Massachusetts Institute of Technology

Access: Phone: (617) 253-7492
Fax: (617) 253-9845
E-mail: globalchange@mit.edu
Web site: http://MIT.EDU/globalchange/

Printed on recycled paper

Methane Fluxes Between Terrestrial Ecosystems and the Atmosphere at Northern High Latitudes During the Past Century: *A retrospective analysis with a process-based biogeochemistry model*

Qianlai Zhuang[*], Jerry M. Melillo[*], David W. Kicklighter[*], Ronald G. Prinn[†], A. David McGuire[‡], Paul A. Steudler[*], Benjamin S. Felzer[*] and Shaomin Hu[*]

Abstract

We develop and use a new version of the Terrestrial Ecosystem Model (TEM) to study how rates of methane (CH_4) emissions and consumption in high-latitude soils of the Northern Hemisphere have changed over the past century in response to observed changes in the region's climate. We estimate that the net emissions of CH_4 (emissions minus consumption) from these soils have increased by an average 0.08 Tg CH_4 yr^{-1} during the 20th century. Our estimate of the annual net emission rate at the end of the century for the region is 51 Tg CH_4 yr^{-1}. Russia, Canada, and Alaska are the major CH_4 regional sources to the atmosphere; responsible for 64%, 11%, and 7% of these net emissions, respectively. Our simulations indicate that large inter-annual variability in net CH_4 emissions occurred over the last century. If CH_4 emissions from the soils of the pan-Arctic region respond to future climate changes as our simulations suggest they have responded to observed climate changes over the 20th century, a large increase in high latitude CH_4 emissions is likely and could lead to a major positive feedback to the climate system.

Contents

[*] The Ecosystems Center, Marine Biological Laboratory, 7 MBL Street, Woods Hole, MA 02543, USA

[†] Joint Program on the Science and Policy of Global Change, Massachusetts Institute of Technology, E40-428, 77 Massachusetts Avenue, Cambridge, MA 02139, USA

[‡] U.S. Geological Survey, Alaska Cooperative Fish and Wildlife Research Unit, University of Alaska Fairbanks, Fairbanks, Alaska, USA

1. INTRODUCTION

Soils have the capacity to both produce and consume methane (CH_4), a powerful greenhouse gas. A special group of soil microorganisms, the methanogens, is responsible for CH_4 production, while another group, the methanotrophs, is responsible for CH_4 consumption. Recent estimates put CH_4 emissions from the world's soils at between 150 and 250 Tg CH_4 yr^{-1} [*IPCC*, 2001], with a quarter to a third of the total emitted from the wet soils of high latitudes [*Walter et al*., 2001a]. Estimates of CH_4 consumption by soil microbes are in the range of 10-30 Tg CH_4 yr^{-1}; an order of magnitude lower than the emission estimates [*IPCC*, 2001]. Most of the CH_4 consumption occurs in the well-drained soils of temperate and tropical areas [*Ridgwell et al.*, 1999].

Terrestrial ecosystems above 45°N have experienced earlier and more dramatic environmental changes from global warming compared with lower-latitude ecosystems, especially in the last decades of the 20th century [*IPCC*, 2001]. These changes include higher mean annual air temperatures, increases in precipitation, and melting of permafrost [*Romanovsky et al*., 2000; *Vitt et al*., 2000]. Changes of CH_4 emissions and consumption due to warming and alterations of hydrology in the region have been measured [e.g., *Friborg et al*., 1997; *Whalen and Reeburgh*, 1992; *West and Schmidt*, 1998]. For example, earlier emissions in response to the early spring thawing in sub-arctic mire ecosystems, and larger emissions due to the increase of active layer thickness in permafrost zones, have been observed [*Whalen and Reeburgh*, 1992; *Moore et al*., 1990*; Dise*, 1993].

Many of the regional and global estimates of CH_4 fluxes between the land and the atmosphere have been based on limited site measurements and simple extrapolation procedures [e.g., *Whalen and Reeburgh*, 1990b; *Whalen et al*., 1991]. Recently, several large-spatial-scale models [e.g. *Cao et al*., 1996; *Liu*, 1996; *Potter et al*., 1996; *Prinn et al*., 1999; *Ridgwell et al*., 1999; *Walter and Heimann*, 2000, *Walter et al*., 2001a,b] have been developed to estimate current and future methane exchanges between the land and the atmosphere. These models have incorporated many of the factors that control CH_4 fluxes and have led to major advances in our understanding net CH_4 fluxes to the atmosphere from northern ecosystems. However the extant models have not dealt with the complex behavior of the freeze-thaw phenomena, i.e., freezing upward from the permafrost boundary as well as downward from the surface [see *Zhuang et al*., 2001; *Goodrich*, 1978a,b] in the northern ecosystems. We built on this solid foundation by explicitly considering freeze-thaw dynamics of permafrost and directly coupling net primary productivity (NPP) to CH_4 dynamics.

To examine the responses of CH_4 fluxes between soils and the atmosphere at high latitudes, we have developed a new methane module and coupled it to our process-based biogeochemistry model, the Terrestrial Ecosystem Model [TEM; *Melillo* 1993; *Zhuang et al.*, 2003]. We estimate the net CH_4 fluxes from the region above 45° N during the 1990s and the contributions of sub-regions to this total flux. We then explore how these net CH_4 fluxes from the high-latitude soils of the Northern Hemisphere have changed from 1900 to 2000.

2. METHODS

2.1 Model Framework

We have developed a daily time-step methane dynamics module (MDM) for TEM that explicitly considers the process of CH_4 oxidation (methanotrophy) as well as CH_4 production (methanogenesis) and the transport of the gas from the soil to the atmosphere. We coupled the MDM module with several extant TEM modules (**Figure 1**a): the core carbon and nitrogen dynamics module [CNDM; TEM, *Zhuang et al*., 2003]; the soil thermal module (STM) that includes permafrost dynamics [*Zhuang et al*., 2001]; and an improved and expanded hydrological module (HM) that simulates water movement across an atmosphere-vegetation-soil continuum. For northern ecosystems, the soil component of this HM module includes the moss, organic soil, and mineral soil layers [*Zhuang et al.*, 2002], and is designed to consider fluctuations in water-table depth.

2.1.1 Methane Module

Fluxes of methane between soils and the atmosphere depend on the relative rates of methane production and oxidation within the soil profile and the transport of methane across the surface of soils. We assume that soils can be separated into upper unsaturated and lower saturated zones according to the water table depth. Methanotrophy (methane oxidation) occurs in the unsaturated zone and methanogenesis (methane production) occurs in the saturated zone. As methanotrophy reduces soil methane concentrations in the unsaturated zone and methanogenesis increases soil methane concentrations in the saturated zone, the resulting concentration gradient causes methane to diffuse from the saturated zone into the unsaturated zone. If the rate of methanogenesis is larger

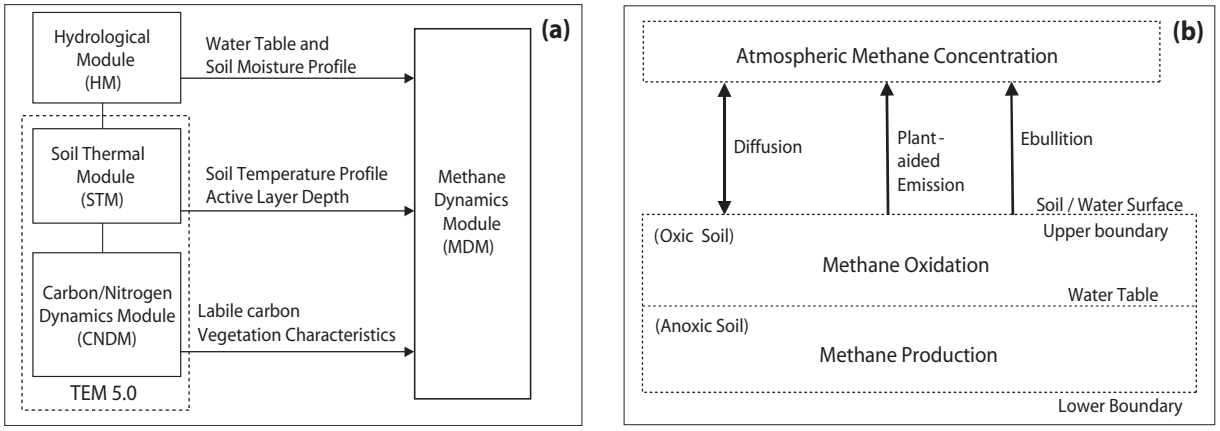

Figure 1. **(a)** The schematic diagram of the new version of a biogeochemistry model (TEM): It contains a soil thermal module [STM; Zhuang et al., 2001], a updated hydrologic module (HM) based on Zhuang et al. [2002], a carbon/nitrogen dynamics module [CNDM] from the previous version of TEM [Zhuang et al., 2003], and a methane dynamics module (MDM). **(b)** The structure of the MDM module: the soil is separated into anaerobic and aerobic zones by water table position, the CH_4 production and oxidation rate are determined with factors described in Appendices A and B, the CH_4 fluxes between soils and the atmosphere are calculated considering different transport pathways described in Appendix C.

than the rate of methanotrophy within the soil profile, such as occurs in wetland soils, methane will be emitted to the atmosphere. There are two other pathways in addition to diffusion that can be important in CH_4 transport to the atmosphere. Soil CH_4 can be transported from deep in sediments and soils through "hollow tubes" running from the roots through the stems of some plants (plant-aided transport). If the water table is above the soil surface, methane can move in bubbles through the overlying water and escape to the atmosphere. This transport process is known as ebullition.

If the rate of methanotrophy is greater than the rate of methanogenesis within the soil profile, then most, if not all, of the methane produced in the saturated zone will be oxidized in the unsaturated zone and little or no CH_4 will be emitted from soils. Indeed, if the rate of methanotrophy is higher than the rate of methanogenesis, a concentration gradient may develop that causes methane to diffuse from the atmosphere into the soil, such as occurs in well-drained upland soils.

To simulate methane dynamics within the soil, we divide the soil column into a layered system with 1 cm increments above and below the water table depth from an upper boundary (i.e., the soil surface or water surface if the water table is above the soil surface) to a lower boundary, which represents the depth of microbial activity (Figure 1b). The lower boundary (L_B) is defined according to the simulated active layer (unfrozen) depth from the soil thermal module. If the active layer depth is deeper than the prescribed lower boundary ($L_{MAXB;}$ see **Table 1**), the L_B is equal to L_{MAXB}; otherwise the L_B is equal to the active layer depth. Within each soil layer, changes in CH_4 concentration are governed by the following equation:

$$\frac{\partial C_M(z,t)}{\partial t} = M_P(z,t) - M_O(z,t) - \frac{\partial F_D(z,t)}{\partial z} - R_P(z,t) - R_E(z,t) \qquad \text{(Eq. 1)}$$

where $C_M(z,t)$ is the soil CH_4 concentration at depth z (cm) and time t (1 hour), $M_P(z,t)$ is the CH_4 production rate, $M_O(z,t)$ is the oxidation rate, $F_D(z,t)$ is the diffusive flux of CH_4 through the soil layer, $R_P(z,t)$ is the plant-aided emissions rate, and $R_E(z,t)$ is the ebullitive emissions rate. The term, $\frac{\partial F_D(z,t)}{\partial z}$, represents the net change in methane concentration resulting from the diffusion of methane into soil layer z from the layer below and the diffusion of methane out of soil layer z into the layer above. The rates of diffusion and emissions calculated for each soil layer within the soil profile are then used to determine the CH_4 flux at the soil or water surface. The CH_4 fluxes ($F_{CH4}(t)$) between the atmosphere and the soils are the total of the fluxes at the soil/water-atmosphere boundary via different transport pathways:

$$F_{CH4}(t) = F_D(z = s,t) + F_P(t) + F_E(t) \qquad \text{(Eq. 2)}$$

where $F_D(z = s, t)$ is the diffusive flux at the interface between the soil surface and the atmosphere, $F_P(t)$ are the plant-aided emissions, and $F_E(t)$ are the ebullitive emissions.

Table 1. Parameterizations of the Methane Module at Calibration Sites for Simulating CH_4 Effluxes in this Study

Parameters [a]	Toolik-D [b]	Toolik-W	SSA-FEN	B-F	Tundra-NS	Tundra-UI	Unit
L_{MAXB}	80	100	250	100	100	100	cm
			Methanogenesis				
M_{GO}	2.6	1.3	2.1	0.4	4.3	4.3	μMh^{-1}
NPP_{MAX}	100	150	250	250	100	100	$gCm^{-2}month^{-1}$
P_{Q10}	8.0	4.6	4.5	10.0	10.0	10.0	--
P_{TR}	25.0	23.0	22.0	7.0	8.0	8.0	°C
			Methanotrophy				
O_{MAX}	35	30	40	1.0	1.0	30	$\mu M\ h^{-1}$
K_{CH4}	5.0	5.0	5.0	15	10.0	5.0	μM
O_{Q10}	3.5	2.2	1.9	1.5	0.8	2.5	--
O_{TR}	14.0	20.0	25.0	5.4	5.0	20.0	°C
MV_{MAX}	1.0	1.0	1.0	1.0	0.9	1.0	% Volume
MV_{MIN}	0.0	0.0	0.0	0.2	0.0	0.0	% Volume
MV_{OPT}	0.5	0.5	0.5	0.6	0.4	0.5	% Volume

[a] See Text or Appendix for the definition of variables

[b] See Table 2 for site name and description

By numerically solving the Eq.1, we obtain $F_D(z = s, t)$ which will be positive if methane diffuses from soils out to the atmosphere and will be negative is methane diffuses from the atmosphere into soils. We determine $F_P(t)$ by integrating the $R_P(z,t)$ across the soil profile from the soil surface to the rooting depth. Similarly, $F_E(t)$ is obtained by integrating $R_E(z,t)$ over the saturation zone. The $F_E(t)$ term will be equal to 0.0 if the water table is not at or above the soil surface.

As both biological activity and transport rates influence our estimates of CH_4 fluxes at the soil/water surface, we describe below how we obtain the terms in equation 1 in more detail.

Methane production. Methane production is modeled as an anaerobic process that occurs in the saturated zone of the soil profile. We estimate hourly methanogenesis ($M_p(z,t)$) within each 1 cm layer of the soil profile as follows:

$$M_P(z,t) = M_{G0} f(S_{OM}(t)) f(M_{ST}(z,t)) f(pH(t)) f(R_X(z,t)) \quad \text{(Eq. 3)}$$

where M_{G0} is the vegetation-specific maximum potential production rate (Table 1); $f(S_{OM}(z,t))$ denotes the effects of methanogenic substrate availability, which is a function of NPP simulated from the CNDM module and is described in section 2.1.4.; $f(M_{ST}(z,t))$ denotes the effects of soil temperature, which is calculated in the STM module; f(pH(t)) represents the effects of soil pH; and $f(R_X(z,t))$ denotes the effects of the availability of electron acceptors which is related to redox potential. Details of the components of Equation 3, except $f(S_{OM}(z,t))$, are presented in Appendix A.

Methane oxidation. Methane oxidation is modeled as an aerobic process that occurs in the unsaturated zone of the soil profile. We estimate hourly methanotrophy ($M_O(z,t)$) within each 1 cm layer of the soil profile as follows:

$$M_O(z,t) = O_{MAX} f(C_M(z,t) f(T_{SOIL}(z,t)) f(E_{SM}(z,t)) f(R_{OX}(z,t)) \quad \text{(Eq. 4)}$$

where O_{MAX} is the vegetation-specific maximum oxidation coefficient (Table 1), that typically ranges between 0.1 and 100 $\mu molm^{-3}s^{-1}$ [*Segers*, 1998]; $f(C_M(z,t))$ is the effect of the soil methane concentration; $f(T_{SOIL}(z,t))$ is the effect of soil temperature, which is calculated in the STM module; $f(E_{SM}(z,t))$ is the effect of soil moisture, which is provided from the HM module; $f(R_{OX}(z,t))$ is the effect of redox potential; z represents the depth (cm) of the soil layer and t represents time (hour). Details of the components of Equation 4 are presented in Appendix B.

Methane transport. In the model, we consider three pathways by which CH_4 can be transported from the site of production to the atmosphere: diffusion through the soil profile ($F_D(z,t)$), plant-aided transport ($R_P(z,t)$) and ebullition ($R_E(z,t)$. Soil diffusion is the dominant transport process, and we assume that it follows Fick's law. Along the diffusion pathway, CH_4 can be oxidized in the unsaturated zone so that it does not reach the atmosphere. In contrast, methane in plant-aided emissions and ebullitions will not undergo oxidation before reaching the atmosphere. We describe, in more detail, how we modeled each of these transport pathways in Appendix C.

2.1.2 Soil Thermal Module

The soil thermal module [STM; *Zhuang et al*., 2001, 2002, 2003] is used to estimate the active layer depth (seasonal thaw depth) and soil temperatures at specified depths within the soil profile based on monthly or daily air temperatures and precipitation. In the module, the vertical soil profile is divided into snow cover, moss (or litter), and four soil layers: upper organic soil, lower organic soil, upper mineral soil, and lower mineral soil. The snow cover and these soil layers have distinct soil thermal conductivities and heat capacities. The module considers two freezing fronts; i.e., freezing upward from the permafrost boundary, as well as freezing downward from the surface. A snow classification system [*Liston and Pielke,* 2000] has been implemented to better characterize the effect of the snow density and thermal conductivity on the soil thermal regime at a large spatial scale. The soil thermal module has been designed to run at a flexible time step (e.g., 0.5 hour, 0.5 day) and several depth steps (e.g., 2 cm, 5cm). The module has been calibrated and validated for major biomes in the Northern Hemisphere in *Zhuang et al*., [2001, 2002] and for different biome types across the globe in *Zhuang et al*. [2003]. In this study, the methane module requires the soil temperatures at each 1 cm depth of the soil layer in addition to the active layer depth of soils. Therefore, we first simulate the soil temperatures for a variable number of depths within the organic and mineral soil layers. The soil temperatures at each 1 cm depth are then obtained through linear interpolation with the simulated soil temperatures for those layers.

2.1.3 Hydrologic Module

In this study, the methane module requires soil moisture estimates for each 1 cm soil layer within the profile and the estimated depth of the water table in wetland soils on a daily basis. We use an updated version of the hydrologic module [HM, *Zhuang et al*., 2002] to provide these estimates. Module improvements include: 1) the consideration of surface runoff when determining

infiltration rates from rain throughfall and snow melt, 2) the inclusion of the effects of temperature and vapor pressure deficit in the determination of canopy water conductance when estimating evapotranspiration, and 3) a more detailed representation of water storage and fluxes within the soil profile of upland soils based on the Richards equation in the unsaturated zone [*Hillel*, 1980]. As the original version of the HM is designed to simulate water dynamics only in upland soils, algorithms have also been added to simulate water dynamics in wetland soils.

For wetlands, the soil profile is divided into two layers: 1) an oxygenated, unsaturated zone; and 2) an anoxic, saturated zone based on the water table depth. The soil water content and the water table depth in these soils are determined using a water-balance approach that considers precipitation, runoff, drainage, snow sublimation, and evapotranspiration. The soil moisture at each 1 cm depth above the water table is modeled with a quadratic function and increases from the soil surface to the position of the water table [*Granberg et al*., 1999]. The detailed description of the updated HM module is documented in Appendix D.

2.1.4 Carbon/Nitrogen Dynamics Module

We assume that the production of root exudates during the growing season enhances methanogenesis by increasing the availability of organic carbon substrate. To capture the effect of spatial and temporal variations in root exudates on methanogenesis, we use net primary productivity (NPP) estimates from the carbon/nitrogen dynamics module (CNDM) of the Terrestrial Ecosystem Model [TEM; *Zhuang et al.*, 2003]. The NPP estimates are used as an indicator for the variations in methanogenic substrate as follows:

$$f(S_{OM}(z,t)) = (1 + \frac{NPP(mon)}{NPP_{MAX}}) f(C_{DIS}(z)) \quad \text{(Eq. 5)}$$

where NPP(mon) is monthly net primary productivity; NPP_{MAX} represents the maximum monthly NPP expected for a particular vegetation type (Table 1); $f(C_{DIS}(z))$ is the relative availability of organic carbon substrate at depth z in the soil profile; and t represents time (hour). While organic substrates associated with fine root mortality are assumed to be available throughout the year, the ratio of NPP(mon) to NPP_{MAX} is used to represent the additional availability of root exudates during the growing season (i.e., NPP greater than 0.0). Hence, the first term on the right-hand side of equation 5 is assumed to equal 1.0 during the dormant season. We assume the simulated monthly NPP remains constant throughout the month. As a result of root mortality, we assume that $f(C_{DIS}(z))$ is equal to 1.0 throughout the rooting zone (i.e., z is above the rooting depth). If z is below the rooting depth, the effect of $f(C_{DIS}(z))$ is assumed to decrease exponentially with depth [*Walter and Heimann*, 2000] as follows:

$$f(C_{DIS}(z)) = e^{\frac{-(z-R_D)}{10.0}} \quad \text{(Eq. 6)}$$

where R_D is rooting depth as determined by soil texture and vegetation type [V*örösmarty et al*., 1989].

Table 2. Site Descriptions, Soil Characteristics, Driving Data, and Observation Data Used to Parameterize and Test the Model

Site Name	Location (Lon./Lat.)	Elevation	Vegetation	Soil and Climate Characteristics	Driving Climate Data	Observed Data	Sources and Comments
Calibration sites for tundra ecosystems							
Moist Tundra on Unalaska Island (Tundra-UI)	167˚W / 53˚N	--	Wet tundra	Air temperature ranged from 5 to 8˚C. Soil pH is 5.7	Climate data from Shemya USAF Base station (52˚43'N, 174˚06'W)	Static chamber measured CH_4 uptake	*Whalen & Reeburgh* [1990a]; http://www.wrcc.dri.edu
Tundra at Toolik Station of Alaska (Toolik-D)	149˚ 36'W / 68˚38'N	760 m	Tussock tundra	Continuous permafrost, short cool summers, long cold winters; the soils unevenly covered with an organic mat 0-30 cm thick, underlain by a silty mineral soil. The maximum depth of thaw is 30-50 cm, soil pH is 5.0	Air temperature and precipitation (1991-96) at the site, winter precipitation use 30-year average values of daily data at arctic village, Alaska station (68˚08'N, 145˚32'W)	Soil temperature at depths 10, 20, & 50 cm, CH_4 fluxes of 1992 and 1993	http://ecosystems.mbl.edu/ARC and http://www.wrcc.dri.edu
Tundra at Toolik Station of Alaska (Toolik-W)	Same as above	760 m	Wet tussock tundra	Vegetation is wet tundra, soil pH is 5.0	Same as above	Soil temperatures at depth 3, 5, 7, 9, and 11cm, CH_4 fluxes from 1994 and 1995 at the ARCSS-LAII site	*King et al*. [1998]; Also see http://www-nsidc.colorado.edu/data/arcss013.html
Tundra at North Slope of Alaska (Tundra-NS)	--	--	Sedge, moss tussock tundra	Predominately saturated soils, continuous permafrost, thick peats	Climate data from NOAA records for Fairbanks Int'l Airport from 1986 to 1991	Static chamber CH_4 uptake	*King et al.* [1989]
Calibration sites for boreal forest ecosystems							
Boreal Forests at Bonanza Creek of Alaska (B-F)	148˚ 15'W / 64˚ 41'N	133 m	Black spruce, feather moss	Pergelic Cryaquepts, pareant material is Alluvium, forest floor depth is 20 cm, intermittent permafrost. The active layer thickness is highly variable. Some years the frozen layer persists at a depth of 140 cm. Soil pH is 5.4	Climate data from National Oceanic and Atmospheric Administration (NOAA) records for Fairbanks International Airport, 6 km south of study site, from 1986 to 1991	CH_4 fluxes from late May to September of 1990	*Whalen et al*. [1991], See http://www.lter.uaf.edu/
Fen at Southern Study Area of BOREAS (SSA-FEN)	105˚ 57'W / 53˚ 57'N	524.7 m	Complex fen with buckbean, sedges, birch, and willow	Depth of peat is 1-3 m. High temperature (>20 ˚C) and vapor pressure deficit (>1.5 kPa). Soil pH is 7.1	Daily temperature and precipitation are from the Canadian AES -Nipawin station from 1994-1996. Vapor pressure from the CRU data for the grid cell	Soil temperatures at 10 and 20 cm depth, daily evapo-transpiration and eddy covariance measurements of CH_4 fluxes for May to October of 1994 and 1995	*Sellers et al.* [1997]; *Newcomer et al.* [2000]; *Suyker et al.* [1996, 1997]
Test sites							
Tundra at Fairbanks of Alaska (Tundra-F)	147˚ 51'W / 64˚ 52'N	158.5 m	Tussock tundra, dominated by *Eriophorum*	Poorly drained soil, underlain permafrost; typical interior Alaska climate, little standing water, soils are saturated during freeze-up. Soil pH is 5.4	Climate data from NOAA records for Fairbanks International Airport, 6 km south of study site, from 1987 to 1990	Three sites of CH_4 emissions observed using chamber techniques from 1987 to 1990	See *Whalen & Reeburgh*, [1992]; *Ojima et al*. [2000]; http://www.nrel.colostate.edu/projects/tragnet/
Fen at Northern Study Area of BOREAS (NSA-FEN)	98˚ 25'W / 55˚ 55'N	218 m	Fen complex with sedge (Carex spp.), moss, moat, and shrubs	Shrub-dominated hummock-hollow; permafrost peat plateau; soil pH ranges from 3.8 to 7.2	Daily temp. & precipitation from Manitoba station of Canadian AES from 1994to 1996. Vapor pressure data from CRU data sets for the grid cell	Soil temperatures at depths 5, 10, 20, 50, and 100 cm; water table depth (1994) and chamber measurements of CH_4 fluxes of May-Sept. 1994 & June-Oct. 1996	See *Newcomer et al.* [2000]; *Bubier et al.* [1995, 2000]

2.2 Methane Module Parameterization

We parameterize the model using measurements of CH_4 fluxes and key soil and climate factors made at six field sites in North America between 53°N to 68.5°N (**Table 2**). Four of the six sites are in the Alaskan tundra and they include both tussock and wet tundra. One of the sites is in the boreal forest of Alaska and another is in the boreal forest of Canada.

We parameterize the methane module by minimizing the differences between observed fluxes and simulated fluxes at the Toolik-D, Toolik-W, and SSA-FEN field sites. For each site, we start the parameterization procedure with an initial set of parameter values determined by a review of the literature. Each individual parameter has been adjusted to be within a range of values provided from the literature review until the root mean square error (RMSE) between the daily simulated and observed CH_4 fluxes was minimized. This procedure is conducted sequentially for all parameters with the result that RMSE for the Toolik-D, Toolik-W, and SSA-FEN parameterizations are 20, 52, and 42 mg CH_4 m^{-2} day^{-1}, respectively.

Unlike the wetland sites, we do not have a daily time series of CH_4 flux data for the other three upland sites. Therefore, we parameterize the methane module so that the difference between the simulated and observed maximum daily CH_4 consumption rate was minimized at these sites. Specifically, we alter the parameters of the methane module until the simulated CH_4 uptake reaches the maximum uptake rate of 0.95, 1.2, and 2.7 mg CH_4 $m^{-2}day^{-1}$ at the B-F, Tundra-NS, and Tundra-UI sites, respectively. Because the meteorological observations of some sites are not available to us, we use climatic data from other sources (see Table 2), and it is possible that this may lead to biases in the parameterization. In addition, our approach of adjusting a single parameter at a time may lead to biases in parameterizations. The site-specific parameters for the methane module are documented in Table 1. The parameterizations are applied to our regional extrapolation for wetlands and uplands of major northern ecosystems including alpine tundra / polar desert, wet tundra, and boreal forests (**Table 3**).

2.3 Model Testing at the Site Level

To test the model and validate our parameterizations, we conduct simulations for a boreal forested wetland site (NSA-FEN) in Canada and a tundra site (Tundra-F) at Fairbanks, Alaska, which are not used for our parameterization process. We compare the simulated daily CH_4 fluxes to observations. The site descriptions, input climate data sets, and observed CH_4 fluxes are described in Table 2. For conducting simulations for the NSA-FEN site, we apply the parameterization of the SSA-FEN site. For the simulations at the Tundra-F site, we apply the parameterization of the Toolik-W site.

Table 3. Parameterizations Applied to Major Ecosystem Types in Northern High Latitudes

Ecosystem	Wetland	Upland
Alpine tundra/polar desert	Toolik-D	Tundra-NS
Wet tundra	Toolik-W	Tundra-UI
Boreal forests	SSA-FEN	B-F

2.4 Regional Simulations Using Geographically Explicit Data

To make spatially and temporally explicit estimates of CH_4 emissions and consumption in the northern high latitudes (above 45°N) with our new version of TEM, we use spatially explicit data of climate, vegetation, and soils from a variety of sources. The model is applied at the spatial resolution of 0.5° by 0.5° (longitude by latitude) and at a daily time step for the period 1900 through 2000.

The non-climate datasets include potential vegetation similar to that described in *Melillo et al*. [1993], and soil texture and elevation described by *Zhuang et al*. [2003]. In addition, we use the dataset of *Matthews and Fung* [1987] to define the distribution of wet soils in the region, and a dataset from the International Geosphere-Biosphere Programme (IGBP) to assign spatially explicit soil-water pH [*Carter and Scholes*, 2000]. The dataset of the fractional inundation of wetlands, which is used to derive the proportions of wetlands and uplands of grid cells, is also taken from *Matthews and Fung* [1987].

The daily climate datasets are derived from the historical monthly air temperature, precipitation, vapor pressure, and cloudiness datasets [*Mitchell et al*, 2003] of the Climatic Research Unit (CRU) of the University of East Anglia in the United Kingdom. We linearly interpolate the monthly air temperature and vapor pressure to daily data using three consecutive month's data. To determine a current month's daily air temperatures, for example, we assume that: 1) the value of day 15 is equal to the current month's mean air temperature; 2) the value of the first day is equal to the average monthly air temperature of the current month and the previous month; and 3) the value of last day is equal to the average monthly air temperature of the current and the next month. The temperatures for the other days are linearly interpolated using values of the first, 15th and last days. To convert monthly precipitation into daily rainfall, we use the statistical algorithm of *Li and Frolking* [1992] and *Liu* [1996]. The algorithm converts the monthly precipitation into a number of rainfall events of different duration and intensity based on air temperature and the statistical results on the correlation of monthly precipitation with the frequency of heavy, intermediate, and small rainfall events.

In the HM module, the evapotranspiration processes are driven by monthly LAI datasets for the period 1982 to 1999 derived from satellite imagery [*Myneni et al*., 1997; 2001]. From 1900 to 1981, we use the LAI of 1982 to represent LAI during this period. We also use the LAI of 1999 to represent LAI during 2000. We assume the LAI is constant within a month.

To develop regional estimates of CH_4 exchange from 1900 to 2000, we simulate the methane dynamics and estimate CH_4 fluxes from both wetland and upland ecosystems in each 0.5° grid cell. These ecosystem-specific CH_4 flux estimates are then area-weighted for each grid cell as defined by the fractional inundation data set of *Matthews and Fung* [1987].

3. RESULTS AND DISCUSSION

3.1 Site-Specific Testing

At the test site Tundra-F, the simulation captures inter-annual and seasonal variations of the net CH_4 emissions. The simulated annual emissions are 12.2, 10.4, 7.6, and 12.1 g CH_4 m^2yr^{-1} for 1987, 1988, 1989, and 1990, respectively compared to observed fluxes of 8.05 ± 2.5, 11.38 ± 2.88, 8.11 ± 1.80, and 13.64 ± 1.20 g CH_4 m^2yr^{-1} for the same years [See *Whalen and Reeburgh*, 1992]. The linear regression statistics show a significant ($P < 0.01$; N = 48 months) relationship between the simulated and observed monthly emissions with $R^2 = 0.77$, slope = 0.75, and intercept = 0.25 g CH_4 m^{-2} $month^{-1}$ (**Figure 2**a). Overall, the simulations tend to have higher emissions compared to observations during the spring of each year (Figure 2b). This discrepancy is probably because that the model simulated an early spring thaw by considering the insulation of snow pack, which led to early CH_4 production for the site. In 1990, the model underestimates the emissions in August and September. This is primarily because the simulated water tables range from 27 to 28 cm, which is deeper than the measured maximum depth of 23 cm. The deeper water table leads to less CH_4 production and emissions.

Similarly, at our test site, NSA-FEN, the model is able to capture the inter-annual and seasonal dynamics of net CH_4 emissions in 1994 and 1996. A linear regression between monthly simulated and observed net emissions is significant ($P < 0.01$; N = 10 months) with $R^2 = 0.90$, slope = 0.70, and intercept = 0.46 g CH_4 m^{-2} $month^{-1}$ (Figure 2a).

The model slightly underestimates the emissions from June to September in 1996 (Figure 2c). Our analyses suggest that the lower emissions in our simulation are primarily due to the lower soil temperatures resulting from the low soil thermal conductivity prescribed for the model. The deviation may be also partially due to the climate data used to drive the model. Due to the lack of *in-situ* meteorological data at the site, data from the Thompson station of the Canadian Atmospheric Environment Service (AES) has been used to drive the model for this analysis.

3.2 Contemporary Regional and Sub-Regional Fluxes

Overall, our simulations estimate that the Pan-Arctic region has been a source of about 51 T g CH_4 yr^{-1} during the 1990s. This estimate is in the same range as a number of other recent estimates that have been made using a variety of approaches (**Table 4**). Differences between our estimates and those of other studies may be a result of using different geographical boundaries or assuming different importance of various ecosystems in contributing methane to the atmosphere. For example, *Walter et al*. [2001b] considered areas above 30° N in developing their regional estimates rather than the 45° N boundary used in this study. Several studies considered only tundra, boreal forests or wetlands when developing their regional estimates. In our study, we estimate that the source strength varies over the Pan-Arctic and that large regions have actually been small net sinks of atmospheric CH_4 (**Figure 3**).

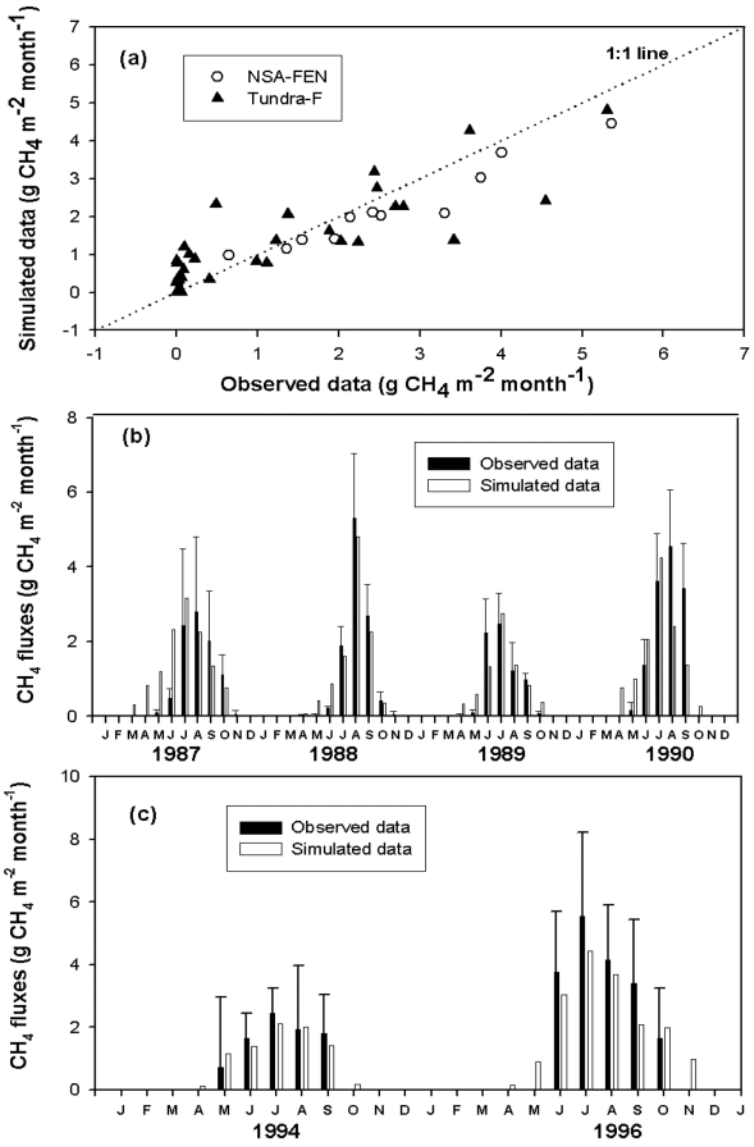

Figure 2. Comparisons between simulated and observed CH_4 emissions at the test sites. **(a)** Scatter plot of observed versus simulated monthly CH_4 emissions for two sites. The open circles indicate data for the NSA-FEN site. The solid triangles indicate data for the Tundra-F site. See Table 2 for site descriptions. The dashed line indicates the 1:1 line for the regressions. For the NSA-FEN site, the statistics are significant ($P < 0.01$, N= 10 months) with $R^2 = 0.90$, slope = 0.70, and intercept = 0.46 g CH_4 m^{-2} $month^{-1}$. Similarly, for the Tundra-F site, the statistics are significant ($P < 0.01$, N = 48 months) with $R^2 = 0.77$, slope = 0.75, and intercept = 0.25 g CH_4 m^{-2} $month^{-1}$. **(b)** Comparison of the observed and simulated monthly CH_4 emissions at the Tundra-F site during the period 1987 to 1990. Error bars indicate the standard deviations for the mean monthly observations from three tussock tundra subsites T1, T2, and T3, see *Whalen and Reeburgh* [1992] for more details. The observed monthly data is aggregated from available daily data from February to December of 1987, January to December of 1988 and 1989, and from May to September of 1990. **(c)** Comparison of the simulated and observed monthly CH_4 emissions at the NSA-FEN test site during 1994 and 1996. The observed daily data are averaged from CH_4 chamber flux measurements at six subsites in 1994 and four subsites in 1996. These subsites represent the range of plant communities, water chemistry, and peatland types found in northern peatlands, including bog, rich fen, poor fen, and collapse scars. The observed monthly data is aggregated from available daily data from May to September of 1994 and from June to October of 1996. Error bars indicate the standard deviations for the mean monthly observations from these subsites.

Table 4. Emissions, Consumption and Net Emissions of Methane from Ecosystem Soils across the Pan-Arctic Region during the 1990s

Studies	**Emissions** (Tg CH_4 yr^{-1})	**Consumption** (Tg CH_4 yr^{-1})	**Net Emissions** (Tg CH_4 yr^{-1})
TEM	57.3	6.3	51.0
Whalen & Reeburgh [1992]	42 ± 26 [a]		
Whalen & Reebugh [1990a]	53 [b]		
Sebacher et al. [1986]	45 - 106 [c]		
Matthews & Fung [1987]	62 [d]		
Crill et al. [1988]	72 [e]		
Walter et al. [2001a]	65 [f]		
Cao et al. [1998]	31 [g]		
Liu [1996]	47 [h]		
Born et al. [1990]		1 - 15 [i]	
Whalen et al. [1991]		0 - 0.8 [j]	
Steudler et al. [1989]		0.3 - 5.1 [k]	
Ridgwell et al. [1999]		5.5 [l]	
Potter et al. [1996]		2.4 [m]	
Chen [2004]			42 - 45 [n]

[a] Estimates for Arctic wet meadow and tussock and shrub tundra
[b] Estimates for global tundra and taiga ecosystems
[c] Estimates for Arctic and boreal wetlands
[d] Estimates for forested and non-forested bogs between 50 - 70ºN
[e] Estimates for undrained peatlands above 40ºN
[f] Estimates for wetlands above 30ºN
[g] Estimates for natural wetlands above 40ºN
[h] Estimates for natural wetlands between 40ºN and 80ºN
[i] Estimates for boreal forests
[j] Estimates for upland and floodplain taiga
[k] Estimates for boreal forests
[l] Estimates for tundra and boreal forests
[m] Estimates for tundra and boreal forests
[n] Estimates based on inverse modeling for the Northern Hemisphere

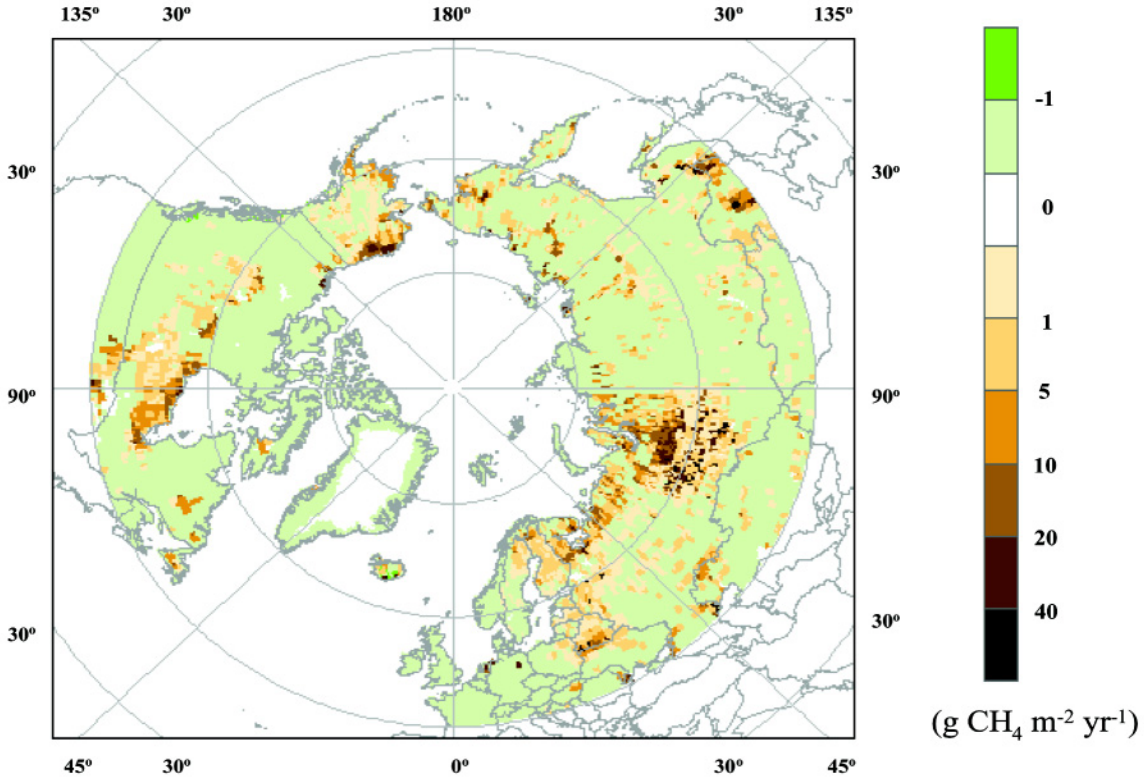

Figure 3. Simulated net CH_4 emissions and consumption in the Pan-Arctic region during the 1990s. Positive values indicate the net CH_4 release to the atmosphere, and negative values indicate the CH_4 uptake from the atmosphere.

Our regional emissions estimate for the Pan Arctic includes wetland areas. This functioned as a net source of CH_4 and upland areas that functioned as a net sink. In our simulations, we estimate that wetlands across the Pan-Arctic emitted about 57 T g CH_4 yr^{-1} during the 1990s. Wetlands within boreal forests have the highest rates of emissions (23 g CH_4 m^{-2} yr^{-1}) but the large areas of wetlands within wet tundra cause these ecosystems to be the largest contributor of atmospheric CH_4.

In addition to the estimates of net CH_4 emissions from wetlands, our simulations estimate that soil microbes in upland areas have consumed about 6 Tg CH_4 yr^{-1} across the Pan-Arctic during the 1990s. This estimate is higher in comparison to most other studies of methane consumption (Table 4), which estimate the consumption rate to be between 0 and 5.5 Tg CH_4 yr^{-1}. An exception is the *Born et al*., [1990] study, which suggested a consumption rate of up to 15 Tg CH_4 yr^{-1}. Upland areas within wet tundra have the highest consumption rates (0.27 g CH_4 m^{-2} yr^{-1}).

The simulated CH_4 emissions and consumption vary across the region depending on the distribution of wetlands as well as spatial climate variability (Figure 3). For the 1990s, our simulations estimate that terrestrial ecosystems within Russia, Canada, and Alaska are the major sources of emissions in the Pan-Arctic, which are contributing 64%, 11%, and 7%, respectively, of the total of 51 T g CH_4 net emissions per year (**Table 5**). Similarly, soils of Russia, Canada, and Alaska consume 38%, 25%, and 5% of the total of 6 Tg CH_4 per year. The West Siberia wetlands in Russia are estimated to emit CH_4 at the rate of 21g CH_4 m^{-2} yr^{-1} for a total of 12 Tg yr^{-1} which is close to the high end of the estimates of 0.3-14 Tg CH_4 yr^{-1} by *Smith et al.* [2004], but lower than the estimate of 26 g CH_4 m^{-2} yr^{-1} by *Friborg et al*. [2003] for this region.

Our simulations indicate that 60% of emissions come from the latitude band of 45-60°N as compared to 40% of total emissions from the region of 60-75°N. This pattern is probably due to the larger areas of wetlands in the southern Pan-Arctic compared to the middle Pan-Arctic as well as to the warmer conditions in the south. The consumption in the southern Pan-Arctic is also two times larger than in the middle Pan-Arctic (**Table 6**), which is primarily due to the larger forest area in the southern Pan-Arctic.

Table 5. Regional Variation in Emissions, Consumption and Net Emissions of Methane during the 1990s

	Russia	**Canada**	**Alaska**	**Pan Arctic**
Emissions (Tg CH_4 yr^{-1})	35.1	7.1	3.8	57.3
Consumption (Tg CH_4 yr^{-1})	-2.3	-1.5	-0.3	-6.3
Net Emissions (Tg CH_4 yr^{-1})	32.8	5.6	3.5	51.0
Area (Mha)	687.4	370.2	65.2	3826

Table 6. Latitudinal Variations in Emissions, Consumption and Net Emissions of Methane during the 1990s

	Northern Pan-Artic (75-90°N)	**Middle Pan-Arctic** (60-75°N)	**Southern Pan-Arctic** (45-60°N)	**Pan-Arctic** (45-90°N)
Emissions (Tg CH_4 yr^{-1})	0.2	23.0	34.0	57.3
Consumption (Tg CH_4 yr^{-1})	–0.2	–2.0	–4.0	–6.3
Net Emissions (Tg CH_4 yr^{-1})	0.0	21.0	30.0	51.0
Area (Mha)	58.7	1473.3	2294.6	3826

3.3 Twentieth Century Trends

During the past century, our simulations estimate that CH_4 emissions have increased at a rate of 0.08 Tg CH_4 yr^{-1}. For the 1980s, the model simulates the increasing trend of emissions (~1.0 Tg CH_4 yr^{-1}), which is consistent with the direct measurements made in Northern Hemisphere [*Dlugokencky et al*., 1994].

While methane consumption rates remain fairly constant throughout the study period, net CH_4 emissions vary from decade to decade (**Table 7**) with relatively large emissions in the 1920-1930s, 1950s and the 1980-1990s. The decadal net emission rates are correlated with decadal variations in climate and its derived variables, namely, soil temperature, water table depth, and NPP. Our analyses indicate net CH_4 emissions are more significantly correlated with air temperature ($R = 0.91$; $P < 0.01$, $N = 10$ decades) than precipitation ($R = 0.64$; $P < 0.01$; $N = 10$ decades). The correlations between decadal net emissions and water table depth, soil temperature, and NPP are significantly ($P < 0.01$) high with R-values of 0.89, 0.92, and 0.82, respectively. These analyses suggest that the climate and its influence on ecosystem production and the soil environment exert strong feedbacks on CH_4 emissions.

Decadal changes of simulated monthly emissions from the 1900s to 1990s show an increasing trend in the magnitude of CH_4 emissions during the growing season (May through September, see **Figure 4**) when root exudates provide additional carbon for methanogenesis. Our simulations show the peak emissions occurred in July, which is consistent with the results of recent inverse modeling studies [*Houweling et al*., 2000; *Chen*, 2004] and other process-based modeling [*Cao et al*., 1996].

Table 7. Decadal Variations in Climate, Net Primary Productivity (NPP), and CH_4 Fluxes for the Past Century in the Pan-Arctic Region

	1900s	1910s	1920s	1930s	1940s	1950s	1960s	1970s	1980s	1990s
CH_4 Emissions ($Tg\ CH_4\ yr^{-1}$)	47.8	48.0	51.5	51.7	50.7	53.4	50.7	50.7	53.8	57.3
CH_4 Consumption ($Tg\ CH_4\ yr^{-1}$)	–6.0	–6.1	–6.1	–6.2	–6.2	–6.2	–6.1	–6.2	–6.2	–6.3
Net CH_4 Emissions ($Tg\ CH_4\ yr^{-1}$)	41.8	41.9	45.4	45.5	44.5	47.2	44.6	44.5	47.6	51.0
Mean Annual Air Temperatures (°C)	–4.0	–4.0	–3.7	–3.5	–3.5	–3.7	–3.7	–3.7	–3.3	–2.9
Mean Annual Precipitation (mm)	471	474	473	478	484	494	505	503	507	505
Mean Annual Soil Temperatures (°C)	–1.2	–1.2	–1.0	–0.9	–0.9	–1.0	–1.0	–1.0	–0.7	–0.5
Mean Annual Water Table Depths (mm)	198.6	198.8	199.5	200.5	200.5	199.6	199.6	200.0	201.5	202.9
NPP ($Pg\ C\ yr^{-1}$)	8.3	8.4	8.3	8.6	8.7	8.7	8.7	8.7	9.0	9.1

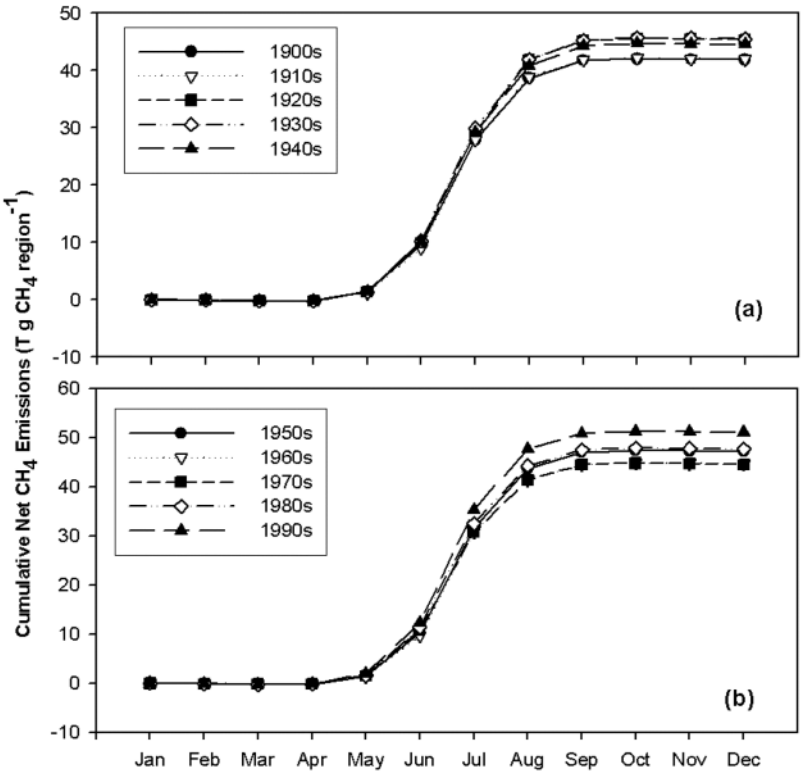

Figure 4. **(a)** Cumulative net CH_4 emissions for each decade from 1900s to 1940s in the Pan-Arctic region. **(b)** Cumulative net CH_4 emissions for each decade from 1950s to 1990s in the Pan-Arctic region.

Our simulations also show that large interannual variability in net CH_4 emissions occurred during the 20th Century (**Figure 5**a,b). For example, our simulations capture the decreasing trend of the CH_4 emissions after the Mount Pinatubo eruption in 1991 (Figure 5c). We estimate that the 50 Tg CH_4 emissions in 1991 decreases to 40 and 45 Tg $CH_4\,yr^{-1}$ in 1992 and 1993, respectively.

This decreasing trend has been observed in the inverse modeling study of *Dlugokencky et al.* [1994], and the modeling study of *Walter et al.* [2001b]. During 1998, there was a large positive anomaly in the global growth rate of atmospheric methane concentrations, *Dlugokencky et al.* [2001] attributed this anomaly in part to increased emissions from wetlands in the high northern latitudes resulting from warm conditions in 1998 due to the strong El Niño phenomena. Our simulation results support this interpretation and indicate that the region released 55 Tg CH_4 in 1998, an amount that is 8-11 Tg higher than emissions in 1999 and 1997.

3.4 Conclusions and Future Directions

In this study, we couple key aspects of soil thermal and hydrological dynamics and carbon dynamics of the terrestrial ecosystems with methane cycling to estimate CH_4 fluxes between the atmosphere and the soils in the Pan-Arctic region. By considering the ability of soils to produce methane in wetland soils and to oxidize methane in both wetland and upland soils, we have developed more comprehensive regional estimates of CH_4 fluxes than provided by earlier studies

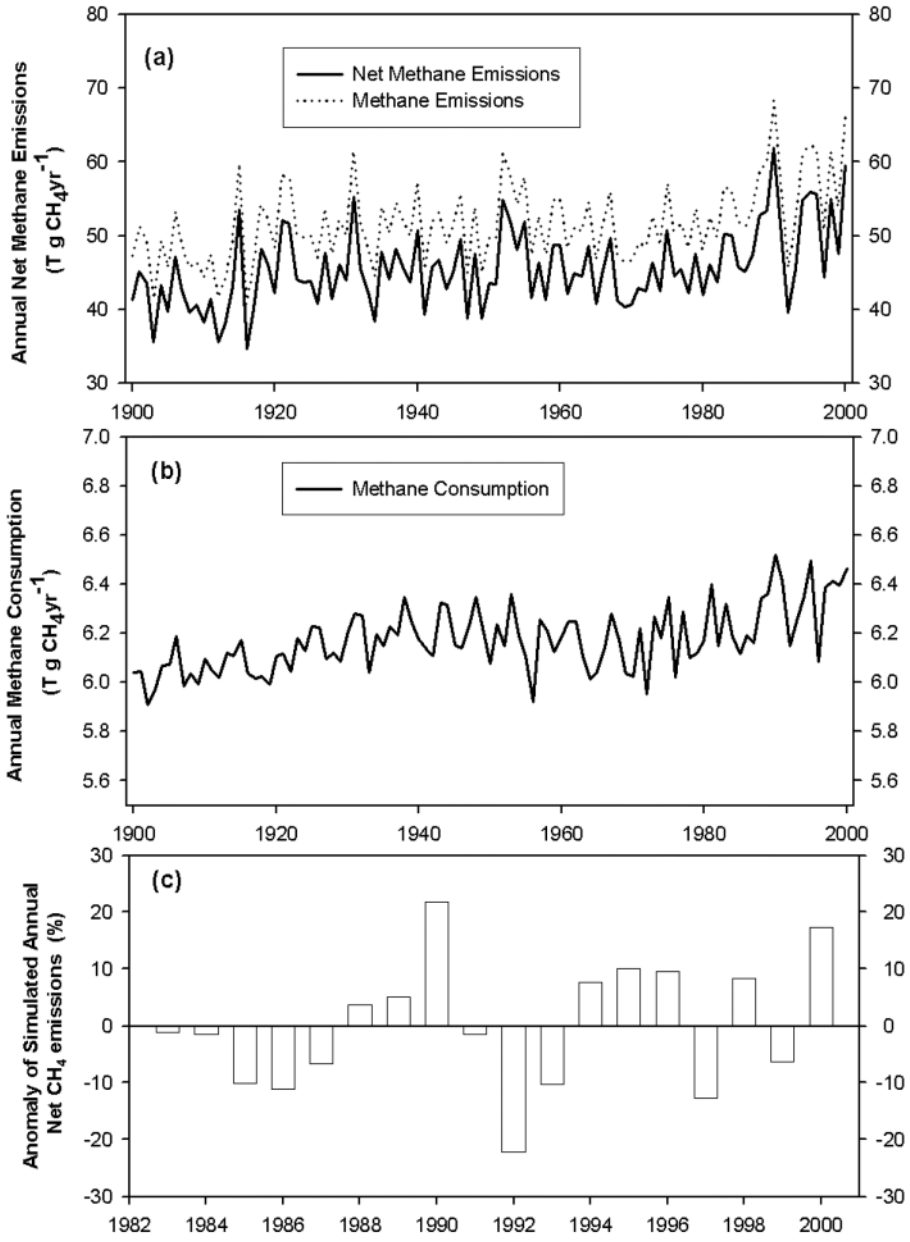

Figure 5. **(a)** Annual net methane emissions from the Pan-Arctic region during the 20th century. **(b)** Annual methane consumption from the Pan-Arctic region during the 20th century. **(c)** Anomaly of simulated net CH_4 emissions in the pan-Arctic region from 1983 to 2000. Anomalies are calculated based on the averaged net CH_4 emissions from 1982 to 2000.

using process-based models or field estimates. Our analyses suggest that CH_4 emissions are more sensitive to changes in climate, particularly air temperature, than consumption such that natural ecosystems may become a larger source of atmospheric CH_4 with future climate change. In addition, our analyses suggest that changes in root exudates associated with climate-induced enhancements in plant productivity may also increase CH_4 emissions. However, reductions in the

area of wetlands in the Pan Arctic region [e.g., *McGuire et al*., in press] as a result of alterations of the hydrological cycle may allow methane consumption by soils to become more important.

Our regional estimates of net CH_4 emissions from natural ecosystems are 10 to 20 percent higher than those estimated from an inverse modeling study based on spatial and temporal changes in atmospheric CH_4 concentrations [*Chen,* 2004]. To help resolve this discrepancy and to better understand the role of natural ecosystems in the global methane budget, it is desirable to couple our spatially explicit estimates of CH_4 fluxes to an atmospheric transport model to simulate seasonal and interannual changes in atmospheric CH_4 concentration. This approach has already been taken with CO_2 fluxes and has proved helpful in evaluating and improving the simulation of the various aspects of the carbon cycle including net carbon storage [*McGuire et al.*, 2000; *Dargaville et al*., 2002; *Zhuang et al.,* 2003].

Acknowledgements

We thanks for invaluable discussions and communications with W. Reeburgh, M. Heimann, S. Frolking, P. Crill, E. Matthews, I. Fung, N. Roulet, T. Christensen, and E. Dlugokencky. This study was supported by a NSF biocomplexity grant (ATM-0120468), the NASA Land Cover and Land Use Change Program (NAG5-6257), and by funding from MIT Joint Program on the Science and Policy of Global Change, which is supported by a consortium of government, industry and foundation sponsors.

4. REFERENCES

Bonan, G. B., Sensitivity of a GCM simulation to subgrid infiltration and surface runoff, *Climate Dynamics,* 12: 279-285, 1996.

Born, M., H. Dorr, and I. Levin, Methane concentration in aerated soils in Wets-Germany, *Tellus 42B,* 58-64, 1990.

Brubaker, K., A. Rango, and W. Kustas, Incorporate radiation inputs into the snowmelt runoff model, *Hydrological Processes,* 10, 1329-1343, 1996.

Bubier, J. L., T. R. Moore, L. Bellisario, N. T. Comer, and P. M. Crill, Ecological controls on methane emissions from a northern peatland complex in the zone of discontinuous permafrost, Manitoba, Canada, *Global Biogeochemical Cycles,* 9(4), 455-470, 1995.

Bubier, J.L., P,M. Crill, and T.R. Moore, Magnitude and Control of Trace Gas Exchange in Boreal Ecosystems. In: *Collected Data of The Boreal Ecosystem-Atmosphere Study*. J. Newcomer, D. Landis, S. Conrad, S. Curd, K. Huemmrich, D. Knapp, A. Morrell, J. Nickeson, A. Papagno, D. Rinker, R. Strub, T. Twine, F. Hall, and P. Sellers (editors). CD-ROM. NASA, 2000.

Celia, M. A., and E. T. Bouloutas, and R. L. Zarba, A general mass-conservative numerical solution for the unsaturated flow equation, *Water Resources Research*, 26(7): 1483-1496, 1990.

Chen, Y., Estimation of methane and carbon dioxide surface fluxes using a 3-D global atmospheric chemical transport model, Ph.D. thesis, Massachusetts Institute of Technology, Cambridge, MA, pp. 180, 2004; available as MIT Center for Global Change Science Report 73 (http://web.mit.edu/cgcs/www/MIT_CGCS_Rpt73.html).

Cao, M., S. Marshall, and K. Gregson, Global carbon exchange and methane emissions from natural wetlands: Application of a process-based model, *J. Geophys. Res*., 101(D9), 14,399-14,414, 1996.

Cao, M., K. Gregson, and S. Marshall, Global methane emission from wetlands and its sensitivity to climate change, *Atmospheric Environment***,** 32(19), 3293-3299, 1998.

Carter, A. J., and R. J. Scholes, SoilData v2.0: Generating a global database of soil properties, *Environmentek CSIR*, South Africa, 2000.

Clapp, R. B. and G. M. Hornberger, Empirical equations for some soil hydraulic properties, *Water Resources Research* 14(4): 601-604, 1978.

Crill, P. M., K. B. Bartlett, R. C. Harriss, E. Gorham, E. S. Verry, D. I. Sebacher, L. Mazdar, and W. Sanner, Methane flux from Minnesota peatlands, *Global Biogeochem. Cycles*, 2, 371-384, 1988.

Dargaville, R. J., M. Heimann, A. D. McGuire, I. C. Prentice, D. W. Kicklighter, F. Joos, J. S. Clein, G. Esser, J. Foley, J. Kaplan, R. A. Meier, J. M. Melillo, B. Moore III, N. Ramankutty, T. Reichenau, A. Schloss, S. Sitch, H. Tian, L. J. Williams, and U. Wittenberg. Evaluation of terrestrial carbon cycle models with atmospheric CO2 measurements: results from transient simulations considering increasing CO2, climate and land-use effects, *Global Biogeochem. Cycles*, 16, 1092, doi: 10.1029/2001GB001426, 2002.

Dise, N. B., Methane emission from Minnesota peatlands: Spatial and seasonal variability, *Global Biogeochem. Cycles*, 7, 123-142, 1993.

Dlugokencky, E. J., K. A. Masaire, P. M. Lang, P. P. Tans, L. P. Steele, and E. G. Nisbet, A dramatic decrease in the growth rate of atmospheric methane in the northern hemisphere during 1992, *Geophysical Research Letters*, 21(1): 45-48, 1994.

Dlugokencky, E. J., B. P. Walter, K. A. Masarie, P. M. Lang, and E. S. Kasischke, Measurements of an anomalous global methane increase during 1998, *J. Geophys. Res*., 28(3), 499-502, 2001.

Fiedler, S., and M. Sommer, Methane emissions, groundwater levels and redox potentials of common wetland soils in a temperate-humid climate, *Global Biogeochemical Cycles* 14(4): 1081-1093, 2000.

Friborg, T., T. R. Christensen, and H. Sogaard, Rapid response of greenhouse gas emission to early spring thaw in a subarctic mire as shown by micrometeorological techniques, *Geophysical Research Letters*, 24(23), 3061-3064, 1997.

Friborg, T., H. Soegaard, T. R. Christensen, C. R. Lloyd, and N. S. Panikov, Siberian wetlands: Where a sink is a source, *Geophys. Res. Lett.*, 30 (21), 2129, doi:10.1029/2003GL017797, 2003.

Frolking, S., M. L. Goulden, S. C. Wofsy, S. -M. Fan, D. J. Sutton, J. W. Munger, A. M. Bazzaz, B. C. Daube, P. M. Crill, J. D. Aber, L. E. Band, X. Wang, K. Savage, T. Moore, and R. C. Harriss, Modeling temporal variability in the carbon balance of a spruce/moss boreal forest, *Global Change Biology* 2: 343-366, 1996.

Goodrich, L. E., Some results of a numerical study of ground thermal regimes. *Proc. 3rd Int. Conf. Permafrost*, Ottawa, Vol. 1, National Research Council of Canada, Ottawa, 29-34, 1978a.

Goodrich, L. E., Efficient numerical technique for one-dimensional thermal problems with phase change, *Int. J. Heat Mass Transfer*, **21**, 615-621, 1978b.

Granberg, G., H. Grip, M. Ottosson Lofvenius, I. Sundh, B. H. Svensson, and M. Nilsson, A simple model for simulation of water content, soil frost, and soil temperatures in boreal mixed mires, *Water Resources Research* 35(12): 3771-3782, 1999.

Hillel, D., *Fundamental of Soil Physics,* Academic Press, INC., Harcourt Brace Jovanovich, Pulblishers, pp. 413, 1980

Houweling, S., F. Dentener, J. Lelieveld, B. Walter, and E. Dlugokencky, The modeling of tropospheric methane: How well can point measurements be reproduced by a global model*? J. of Geophysical Research*, 105(D7): 8981-9002, 2000.

IPCC, *Climate Change 2001*: *The Scientific Basis*. Contribution of Working Group I to the Third Assessment Report of the Intergovernmental Panel on Climate Change [Houghton, J. T., Y. Ding, D. J. Groggs, M. Noguer, P. J. van der Linden, X. Dai, K. Maskell, and C. A. Johnson (eds.)]. Cambridge University Press, Cambridge, United Kingdom and New York, NY, USA, 881pp, 2001.

King, S. L., P. D. Quay, and J. M. Lansdown, The $^{13}C/^{12}C$ kinetic isotope effect for soil oxidation of methane at ambient atmospheric concentrations, *J. of Geophy. Res*., 94, D15, 18,273-18277, 1989.

King, J., W. Reeburgh, and S. Regli, *Methane flux data, Alaska North Slope, 1994-1996.* Boulder, CO: National Snow and Ice Data Center. Digital media, 1998.

Li, C., and S. Frolking, Simulation of N_2O emission from soil by DNDC model with generalized climate scenarios, Report, University of New Hampshire, Durham, New Hampshire, 1992.

Liston, G. E., and Pielke, R. A., A climate version of the regional atmospheric modeling system, *Theor. Appl. Climatol*., **66**, 29-47, 2000.

Liu, Y., Modeling the emissions of nitrous oxide (N_2O) and methane (CH_4) from the terrestrial biosphere to the atmosphere, Ph.D. thesis, MIT, pp. 219, 1996.

Matthews, E., and I. Fung, Methane emissions from natural wetlands: Global distribution, area, and environmental characteristics of sources, *Global Biogeochem. Cycles*, 1, 61-86, 1987.

McClaugherty, C. A., J. D. Aber, and J. M. Melillo, The role of fine roots in the organic matter and nitrogen budgets of two forested ecosystems, *Ecology*, 63(5), 1481-1490, 1982.

McGuire, A.D., M. Apps, F.S. Chapin III, R. Dargaville, M.D. Flannigan, E.S. Kasischke, D. Kicklighter, J. Kimball, W. Kurz, D.J. McCrae, K. McDonald, J. Melillo, R. Myneni, B.J. Stocks, D.L. Verbyla, and Q. Zhuang. Canada and Alaska. Chapter 9 in *Land Change Science: Observing, Monitoring, and Understanding Trajectories of Change on the Earth's Surface*. Dordrecht, Netherlands, Kluwer, 2004, in press.

McGuire, A. D., J. M. Melillo, J. T. Randerson, W. J. Parton, M. Heimann, R. A. Meier, J. S. Clein, D. W. Kicklighter, and W. Sauf. Modeling the effects of snowpack on heterotrophic respiration across northern temperate and high latitude regions: comparison with measurements of atmospheric carbon dioxide at high latitudes. *Biogeochemistry*, 48, 91-114, 2000.

Melillo, J. M., McGuire, A. D., Kicklighter, D. W., Moore III, B., Vorosmarty, C. J., and Schloss, A. L., Global climate change and terrestrial net primary production, *Nature*, 63, 234-240, 1993.

Mitchell, T.D., Carter, T.R., Jones, P.D., Hulme, M., New, M., A comprehensive set of high-resolution grids of monthly climate for Europe and the globe: the observed record (1901-2000) and 16 scenarios (2001-2100), *Journal of Climate*, submitted, 2003.

Moore, T. R., N. Roulet and R. Knowles, Spatial and temporal variations of methane flux from subarctic/northern boreal fens, *Global Biogeochemical Cycles*, 4, 26-49, 1990.

Myneni, R. B., Keeling, C. D., Tucker, C. J., Asrar, G. and Nemani, R. R., Increased plant growth in the northern high latitudes from 1981-1991, *Nature*, 386, 698-701, 1997.

Myneni, R.B, J. Dong, C.J. Tucker, R.K. Kaufmann, P.E. Kauppi, J. Liski, L. Zhou, V. Alexeyev, and M.K. Hughes, A large carbon sink in the woody biomass of northern forests, *Proc. Natl. Acad. Sci. USA*., 98(26), 14784-14789, 2001.

Newcomer, J., D. Landis, S. Conrad, S. Curd, K. Huemmrich, D. Knapp, A. Morrell, J. Nickeson, A. Papagno, D. Rinker, R. Strub, T. Twine, F. Hall, and P. Sellers, eds. *Collected Data of The Boreal Ecosystem-Atmosphere Study*. NASA. CD-ROM. NASA, 2000.

Ojima, Dennis, A. Mosier, S.J. DelGrosso, and W.J. Parton. TRAGNET analysis and synthesis of trace gas fluxes, *Global Biogeochemical Cycles* 14:995-997, 2000.

Potter, C. S., E. A. Davison, L. V. Verchot, Estimation of global biogeochemical controls and seasonality in soil methane consumption, *Chemosphere*, 32: 2219-2246,1996.

Press, W. H., B. P. Flannery, S. A. Teukolsky, and W. T. Vetterling, *Numerical Recipes in C, the Art of Scientific Computing*, Cambridge University Press, pp. 735, 1990.

Prinn, R.G., H.D. Jacoby, A.P. Sokolov, C. Wang, X. Xiao, Z. Yang, R. Eckaus, P.H. Stone, A.D. Ellerman, J. Melillo, J. Fitzmaurice, D. Kicklighter, Y. Liu & G. Holian, Integrated Global System Model for Climate Policy Assessment: Feedbacks and Sensitivity Studies, *Climatic Change***,** 41(3/4), 469-546, 1999.

Ridgwell, A. J., S. J. Marshall and K. Gregson, Comsumption of atmospheric methane by soils: A process-based model, *Global Biogeochemical Cycles 13*(1): 59-70,1999.

Romanovsky, V. E., Osterkamp, T. E., Sazonova, T. S., Shender, N. I., and V. T. Balobaev, Past and Future Changes in Permafrost Temperatures Along the East Siberian Transect and an Alaskan Transect, *Trans. AGU*, 81(48), F223-F224, 2000.

Sebacher, D. J., R. C. Harriss, K. B. Bartlett, S. M. Sebacher, and S. S. Grice, Atmospheric methane sources: Alaskan tundra, an alpine fen and a subarctic boreal marsh, *Tellus, Ser. B.*, 38, 1-10, 1986.

Sellers, P. J., F. G. Hall, R. D. Kelly, A. Black, D. Baldocchi, J. Berry, M. Ryan, K. Jon Ranson, P. M. Crill, D. P. Lettenmaier, H. Margolis, J. Cihlar, J. Newcomer, D. Fitzjarrald, P. G. Jarvis, S. T. Gower, D. Halliwell, D. Williams, B. Goodison, D. E. Wickland, and F. E. Guertin, BOREAS in 1997: Experiment overview, scientific results, and future directions. *J. Geophys. Res*. 102 D24, 28731-28769, 1997.

Segers, R., and S. W. M. Kengen, Methane production as a function of anerobic carbon mineralization: A process Model, *Soil Biology & Biochemistry* 30(8/9): 1107-1117, 1998.

Segers, R., Methane production and methane consumption: a review of processes underlying wetland methane fluxes, *Biogeochemistry* 41: 23-51, 1998.

Smith, L. C., G. M. MacDonald, A. A. Velichko, D. W. Beilman, O. K. Borisova, K. E. Frey, K. V. Kremenetski, and Y. Sheng, Siberian peatlands a net carbon sink and global methane source since the early Holocene, *Science*, 303, 353-356, 2004.

Steudler, P. A., R. D. Bowden, J. M. Melillo, and J. D. Aber, Influence of nitrogen fertilization on methane uptake in temperate forest soils, *Nature*, 341, 314-316, 1989.

Suyker, A. E., S. B. Verma, R. J. Clement, and D. P. Billesbach, Methane flux in a boreal fen: Season-long measurement by eddy correlation, *J. Geophys. Res.*, 101, 28,637-28647, 1996.

Suyker, A. E., S. B. Verma, and T. J. Arkebauer, Season-long measurement of carbon dioxide exchange in a boreal fen, *J. Geophys. Res*., 102, 29,021-29,028, 1997.

Thornton, P. E., *Biome-BGC version 4.1.1*, Numerical Terradynamics Simulation Group (NTSG), School of Forestry, University of Montana Missoula, MT 59812, 2000.

Tian, H., J. M. Melillo, D. W. Kicklighter, A. D. McGuire, and J. Helfrich, The sensitivity of terrestrial carbon storage to historical climate variability and atmospheric CO_2 in the United States, *Tellus* 51B(2): 414-452, 1999.

Vitt, H.D., L.A. Halsey, and S.C. Zoltai, The chaning landscape of Canada's western boreal forest: The current dynamics of permafrost, *Can. J. For. Res.*, 30:283-287, 2000.

Vorosmarty, C. J., B. Moore III, A. L. Grace, M. P. Gildea, J. M. Melillo, B. J. Peterson, E. B. Rastetter, and P. A. Steudler, Continental scale models of water balance and fluvial transport: an application to South America, *Global Biogeochemical Cycles*, **3**(3), 241-265, 1989.

Walter, B. P., and M. Heimann, A process-based, climate-sensitive model to derive methane emission from natural wetlands: Applciation to five wetland sites, sensitivity to model parameters, and climate, *Global Biogeochemical Cycles*, 14(3): 745-765, 2000.

Walter, B. P., M. Heimann, and E. Matthews, Modeling modern methane emissions from natural wetlands 1. Model description and results, *J. Geophys. Res*., 106(D24), 34,189-34,206, 2001a.

Walter, B. P., M. Heimann, and E. Matthews, Modeling modern methane emissions from natural wetlands 2. Interannual variations 1982-1993, *J. Geophys. Res.*, 106(D24), 34,207-34,219, 2001b.

Waring, R. H., and Running S. W., *Forest ecosystems, analysis at multiple scales*, second edition, Academic Press, pp. 370, 1998.

Whalen, S., W. S. Reeburgh, and K. S. Kizer, Methane consumption and emission by taiga, *Global Biogeochemical Cycles*, 5(3): 261-273, 1991.

Whalen, S. C., and W. S. Reeburgh, Consumption of atmospheric methane by tundra soils, *Nature*, 346, 160-162, 1990a.

Whalen, S. C., and W. S. Reeburgh, A methane flux transect along the trans-Alaska pipeline haul road, *Tellus, 42B*, 237-249, 1990b.

Whalen, S. C., and W. S. Reeburg, Interannual variations in tundra methane emissions: A four-year time series at fixed sites, *Global Biogeochem. Cycles*, 6, 139-159, 1992.

West, A. E., and S. K. Schmidt, Wetting stimulates atmospheric CH_4 oxidation by alpine soil, *FEMS Microbiol. Ecol.*, 25, 349-353, 1998.

Zhang, Y., C. Li, C. C. Trettin, and H. Li, and G, Sun, An integrated model of soil hydrology, and vegetation for carbon dynamics in wetland ecosystems, *Global Biogeochemical Cycles* 16(4): 1061, doi:10.1029/2001GB001838, 2002.

Zhuang, Q., V. E. Romanovsky, A. D. McGuire, Incorporation of a permafrost model into a large-scale ecosystem model: Evaluation of temporal and spatial scaling issues in simulating soil thermal dynamics, *J. Geophys. Res*., 106, D24, 33,649-33,670, 2001.

Zhuang, Q., A. D. McGuire, K. P. O'Neill, J. W. Harden, V. E. Romanovsky, J. Yarie. Modeling the soil thermal and carbon dynamics of a fire chronosequence in Interior Alaska, *J. Geophy. Res.*, 107, D1, 8147, doi:10.1029/2001JD001244, 2002. [Printed 108(D1), 2003].

Zhuang, Q., A. D. McGuire, J. M. Melillo, J. S. Clein, R. J. Dargaville, D. W. Kicklighter, R. B. Myneni, J. Dong, V. E. Romanovsky, J. Harden, and J. E. Hobbie, Carbon cycling in extratropical terrestrial ecosystems of the Northern Hemisphere during the 20th Century: A modeling analysis of the influences of soil thermal dynamics, *Tellus*, 55B, 751-776, 2003.

APPENDIX A. METHANE PRODUCTION

Methane production occurs in the saturated zone of soils. We model its rate with Equation 3 as a function of carbon substrate availability, soil thermal conditions, soil pH and soil redox potentials. The influence of carbon substrate availability is documented in section 2.1.4. Here we describe, in more detail, the influence of soil thermal conditions, soil pH conditions, and soil redox potentials on the production rate of methane.

A1. Effects of Soil Temperatures

We assume the hourly methane production rate increases logarithmically with soil temperature based on *Walter and Heimann* [2000]:

$$f(M_{ST}(z,t) = P_{Q10}^{\frac{T_{SOIL}(z,t)-P_{TR}}{10}} \quad \text{(Eq. A1)}$$

where $T_{SOIL}(z,t)$ is the hourly (t) soil temperature, which is simulated in the STM module for each 1 cm depth (z) of the soils; P_{TR} is the reference temperature for methanogenesis and varies with vegetation type (Table 1), and P_{Q10} is a vegetation-specific coefficient (Table 1).

A2. Soil pH Effects on Methanogenesis

The effect of soil pH on methane production is modeled following *Cao et al*. [1996] as:

$$f(pH) = \frac{(pH - pH_{MIN})(pH - pH_{MAX})}{(pH - pH_{MIN})(pH - pH_{MAX}) - (pH - pH_{OPT})^2} \quad \text{(Eq. A2)}$$

where pH is the soil pH value at the site, pH_{MIN} is the minimum pH, pH_{MAX} is the maximum pH, and pH_{OPT} is the optimum pH for methane production. We assume values of 5.5, 9.0 and 7.5 for pH_{MIN}, pH_{MAX} and pH_{OPT}, respectively, for all soils.

A3. Redox Potential Effects

Redox potential (E_{HL}) is used to model the relative availability of electron acceptors (e.g., O_2, NO_3^-, SO_4^{-2}, Fe^{+3}, Mn^{+4}), which suppress methanogenesis [*Seger and Kengen,* 1998]. The effects of redox potential on CH_4 production is modeled for each 1 cm depth (z) following *Zhang et al.* [2002] and *Fiedler and Sommer* [2000]:

$$f(R_x(z,t) = 1.0 \text{ if } E_{HL} \le -200; \quad \text{(Eq. A3.1a)}$$

$$f(R_x(z,t) = -0.01 \times E_{HL} - 1.0 \text{ if } E_{HL} \ge -200 \text{ and } E_{HL} \le -100 \quad \text{(Eq. A3.1b)}$$

$$f(R_x(z,t) = 0.0 \text{ if } E_{HL} \ge -100; \quad \text{(Eq. A3.1c)}$$

where E_{HL} is estimated redox potential (mv day^{-1}).

Following *Zhang et al*. [2002] and *Seger and Kengen* [1998], we model changes in E_{HL} as a function of the root distribution, the fraction of water filled pore space, and the water table position at the site:

$$\frac{dE_{HL}(z)}{dt} = C_R \times (A_L - 1.0) \text{ If the depth z is in saturated zone} \quad \text{(Eq. A3.2a)}$$

$$\frac{dE_{HL}(z)}{dt} = C_R \times (A_L + 1.0 - F_W(z)) \text{ If depth z is in the unsaturated zone} \quad \text{(Eq. A3.2b)}$$

$$A_L = F_{CA} \times P_A \times R_{LD} \quad \text{(Eq. A3.3)}$$

where, C_R is the change rate of soil redox potential under saturated conditions, $F_W(z)$ is the fraction of water filled pore space, the F_{CA} is the cross-sectional area of a typical fine root, P_A is a scalar for the degree of gas diffusion from root to atmosphere, and R_{LD} is the fine root length density. We assume that C_R is 100 mv day^{-1}, F_{CA} is 0.0013 m^2, and R_{LD} is 10 m m^{-2} [See *McClaugherty et al.*, 1982] for all ecosystems. We assume P_A is 1.0 for forested ecosystems and 0.5 for other ecosystems. The HM determines $F_W(z)$ for each 1 cm depth based on soil moisture and the porosity of the moss or litter layer, the upper and lower organic soil layer, and the upper and lower mineral soil layers [See *Zhuang et al*., 2002].

APPENDIX B. METHANE OXIDATION

Methane oxidation occurs in upland soils and the unsaturated zone of wetland soils. The oxygenase pathway of methane oxidation dominates methanotrophy in terrestrial ecosystems. We model the oxidation rate as a function of soil CH_4 concentration, which may be supplied either from the atmosphere or methanogenesis in the soil. Other factors include soil temperature, soil moisture, and soil redox potential in Equation 4. Below we describe in more detail the influence in each factor of this equation.

B1. Effects of CH_4 Concentrations

We assume the effect of the CH_4 substrate on oxidation follows Michaelis-Menten kinetics:

$$f(C_M(z,t) = \frac{C_M(z,t)}{K_{CH4} + C_M(z,t)} \quad \text{(Eq. B1)}$$

where $C_M(z,t)$ is soil CH_4 concentration at depth z and time t and K_{CH4} is the vegetation-specific half saturation constant for CH_4 concentrations (Table 1). Typical values of K_{CH4} constants range between 1-66.2 μM. The concentrations of methane in the soil depend on the ability of methane to move through the soil profile. We discuss the transport of methane through the soil profile in Appendix C.

B2. Effects of Soil Temperature

Based on *Walter and Heimann* [2000], we assume the hourly oxidation rate increases logarithmically with soil temperature:

$$f(T_{SOIL}(z,t)) = O_{Q10}^{\frac{T_{TSOIL}(z,t)-O_{TR}}{10}} \quad \text{(Eq. B2)}$$

where $T_{SOIL}(z,t)$ is the hourly (t) soil temperature, which is simulated in the STM module for each 1 cm depth (z) of the soil; O_{TR} is the reference soil temperature (^oC) and varies with vegetation type (Table 1); and O_{Q10} is a vegetation-specific coefficient (Table 1).

B3. Effects of Soil Moisture

We assume the effect of soil moisture on methane oxidation is similar to the effect of soil moisture on soil carbon decomposition [See *Tian et al*., 1999]. Therefore, we model the influence of volumetric soil moisture on methanotrophic microbial activity as:

$$f(E_{SM}(z,t)) = \frac{(M_V - M_{V\min})(M_V - M_{V\max})}{[(M_V - M_{V\min})(M_V - M_{V\max})] - (M_V - M_{Vopt})^2} \quad \text{(Eq. B3)}$$

where M_{vmin}, M_{vopt}, and M_{vmax} are the minimum, optimum, and maximum volumetric soil moistures for the methanotrophic reaction, respectively, and vary with vegetation types (Table 1); M_V is the soil moisture at each 1 cm depth of the soil simulated in the HM module.

B4. Effects of Redox Potential

Redox potential (E_{HL}) is used to model the relative availability of electron acceptors (e.g., O_2, NO_3^-, SO_4^{-2}, Fe^{+3}, Mn^{+4}) on methane oxidation. Oxygen in the soil is the primary electron acceptor for this process [*Seger*, 1998]. However, methane oxidation may still occur under anaerobic conditions (E_{HL} less than 300 mv), if alternative electron acceptors are available. To simulate these effects, we use the relationship between redox potential and methane oxidation described by *Zhang et al.* [2002]:

$$f(R_{OX}(z,t)) = 0.0 \text{ if } E_{HL} < -200 \quad \text{(Eq. B4a)}$$

$$f(R_{OX}(z,t)) = 0.0075E_{HL} + 1.5 \text{ if } -200 \le E_{HL} \le -100 \quad \text{(Eq. B4b)}$$

$$f(R_{OX}(z,t)) = \frac{1}{1200}E_{HL} + \frac{5}{6} \text{ if } -100 < E_{HL} \le 200 \quad \text{(Eq. B4c)}$$

$$f(R_{OX}(z,t)) = 1.0 \text{ if } E_{HL} > 200 \quad \text{(Eq. B4d)}$$

where $f(R_{OX}(z,t)$ is the effect of redox potential at depth z (cm) and time t (hour), and E_{HL} is the estimated redox potential. The calculation of E_{HL} is described in section A3.

APPENDIX C. METHANE TRANSPORT

The atmosphere, vegetation, and soils are treated as a continuum for the movement of methane from soils to the atmosphere. This movement can occur via three different pathways: diffusion, plant-aided emissions, and ebullition. In upland soils, we assume that diffusion of atmospheric methane into soils is the sole method of moving methane through the soil. However, in wetland soils, we assume that all three pathways are important. Here we describe, in more detail, how we estimate the transport of methane through these pathways and how this transport influences our estimates of methane fluxes from the soil to the atmosphere.

C1. Methane Diffusion

We assume that diffusion of methane occurs throughout the soil profile based on the concentration gradient of methane within the soil following Fick's law through coarse soil pores:

$$F_D(z,t) = -D(z)\frac{\partial C_M(z,t)}{\partial z} \qquad \text{(Eq. C1)}$$

where $F_D(z,t)$ is the diffusive flux, and $C_M(z,t)$ is the methane concentration at depth z (cm) and time t (hour). The diffusion coefficient, D(z) in units of mol cm^{-2} h^{-1}, depends on water content and soil texture. We assume a maximum diffusion rate of 0.132×10^{-4} cm^{-2} s^{-1} under saturated conditions and a rate of 0.132 cm^{-2} s^{-1} under unsaturated conditions. This diffusion rate is reduced with increases in silt and clay content of the soil. The $F_D(z,t)$ for each 1 cm depth can be deduced simultaneously from Equation C1 and Equation 1 using the Crank-Nicolson method [*Press et al.*, 1990]. The concentration change at the lower boundary (L_B) is set to zero. The concentration at the soil surface (or water surface if the water table is at or above the soil surface) is set to 0.076 μM to represent the atmospheric CH_4 concentration. As methane may be oxidized as it moves through the unsaturated zone of the soil profile, only diffusion from the soil surface contributes to methane fluxes to the atmosphere as $F_D(z=s, t)$.

C2. Plant-Aided Transport

The root systems of some plants also provide a more direct conduit for methane produced at depth in the soil to reach the atmosphere. As described in *Walter and Heimann* [2000], the rate of methane ($R_p(z,t)$) removed from a soil layer through vegetation roots is modeled as a function of an index of vegetation growth rate ($f_{grow}(t)$), and the quality of plant-mediated transport at a site based on vegetation type and plant density (T_{veg}). We assume T_{veg} equals 0.5 for tundra ecosystems, and 0.0 for boreal forests. In addition, we use the daily mean temperature at 20 cm depth below ground, instead of the 50 cm depth used by *Walter and Heimann* [2000] to calculate the vegetation growth rate index. The plant-aided CH_4 fluxes ($F_P(t)$) is obtained by integrating the $R_p(z,t)$ calculated for each 1 cm soil layer from the soil surface to the rooting depth. The rooting depth is determined from vegetation type and soil texture based on *Vörösmarty et al.* [1989].

C3. Methane Ebullition

The formation of bubbles in the soil profile allows methane to be transported through the soil more rapidly than would be predicted by diffusion alone. Following *Walter and Heimann* [2000], the loss of methane through bubbles ($R_E(z,t)$) from a soil layer at depth z and at time t is modeled as a function of CH_4 concentrations $C_M(z,t)$. In the layers above the water table, the $R_E(z,t)$ is 0.0. In the layers below the water table depth, bubbles are assumed to reach the water table within 1 hour. If the water table is at or above the soil surface, ebullition is assumed to contribute to methane fluxes to the atmosphere as $F_E(t)$. The ebullitive flux $F_E(t)$ is obtained by integrating $R_E(z,t)$ over the whole water-saturated zone between the water table depth and the lower boundary of the soil. If the water table is below the soil surface, methane in bubbles adds to the methane concentration in the soil layer just above the water table and methane continues to diffuse upward. In this case, $F_E(t)$ equals 0.0.

APPENDIX D. UPDATED HYDROLOGIC MODULE

The hydrologic module [*Zhuang et al*. 2002] has been revised to be appropriate for the both upland and wetland soils. The revisions include improvements in the simulation of infiltration (I_F), evapotranspiration of the vegetation canopy (E_V), soil surface evaporation (E_S), and soil sublimation (S_S). In addition, soil moisture dynamics are represented in greater detail and algorithms have been added for simulating water content and water table depth for wet soils based on *Granberg et al*. [1999].

D1. Infiltration from the Soil Surface to the Soil (I_F)

The liquid water from rain throughfall or snowmelt either infiltrates into the soil column or is lost as surface runoff. In *Zhuang et al*. [2002], all liquid water reaching the soil surface has been assumed to infiltrate into the soil column. In this study, we add algorithms to estimate surface runoff and subtract this estimate from rain throughfall and snowmelt to estimate infiltration (I_F). Following *Bonan* [1996], surface runoff is calculated using the Dunne runoff or the Horton runoff depending on whether the soil surface is saturated.

D2. Evapotranspiration from the Vegetation Canopy (E_V)

The evapotranspiration rate from the vegetation canopy (E_V) is modeled using the Penman-Monteith approach [*Zhuang et al*., 2002]. We have modified the calculation of the canopy water conductance (G) to include the effects of air temperature and vapor pressure deficit on G in addition to the effects of leaf water potential. In addition, the algorithms are implemented at a daily time step rather than the monthly time step used in *Zhuang et al*. [2002].

A simplified equation of *Waring and Running* [1998] has been adopted to model the canopy water conductance (G):

$$G = g_{\max} f(A_T) f(VPD) f(\psi) \quad \text{(Eq. D2.1)}$$

where g_{max} is the maximum canopy conductance (mms^{-1}), $f(A_T)$ is the effect of air temperature (A_T) on the canopy conductance, f(VPD) is the effect of the vapor pressure deficit (VPD in Mbar), and $f(\psi)$ is the effect of leaf water potential(*lwp* in MPa). We set g_{max} to be 3.5, 13.5, and 21.2 for alpine tundra, wet tundra, and boreal forests, respectively. The effects of air temperature on canopy conductance are calculated following [*Thornton*, 2000]:

$f(A_T) = 0.0$ if $A_T < -8.0^o$ C (Eq. D2.2a)

$f(A_T) = 1.0 + 0.125 \times A_T$ if $-8.0^o < AT < 0.0^o$ C (Eq. D2.2b)

$f(A_T) = 1.0$ if $A_T > 0.0^o$ C (Eq. D2.2a)

The effects of vapor pressure deficit on canopy conductance are calculated as:

$f(VPD) = 0.0$ if $VPD > VPD_{close}$ (Eq. D2.3a)

$$f(VPD) = \frac{VPD_{close} - VPD}{VPD_{close} - VPD_{open}} \text{ if } VPD_{open} < VPD < VPD_{close} \quad \text{(Eq. D2.3b)}$$

$f(VPD) = 1.0$ if $VPD < VPD_{open}$ (Eq. D2.3c)

where VPD_{close} is the vapor pressure deficit at complete conductance reduction, and VPD_{open} is the vapor pressure deficit at the start of canopy conductance reduction. We assume VPD_{close} is 41.0 Mbar and VPD_{open} is 9.3 Mbar for all vegetation types.

The effects of leaf water potential (*lwp*) on canopy conductance are calculated in a similar manner:

$f(\psi) = 0.0$ if $lwp < \psi_{close}$ (Eq. D2.4a)

$$f(\psi) = \frac{\psi_{close} - lwp}{\psi_{close} - \psi_{open}} \text{ if } \psi_{close} < lwp < \psi_{open} \quad \text{(Eq. D2.4b)}$$

$f(\psi) = 0.0$ if $lwp > \psi_{open}$ (Eq. D2.4c)

where ψ_{close} is the leaf water potential at complete conductance reduction, and ψ_{open} is the leaf water potential at the start of conductance reduction. We assume that ψ_{close} is –2.3 MPa and ψ_{open} is 0.6 MPa for all vegetation types.

D3. Evaporation from the Soil Surface (E_S)

The algorithms used to calculate evaporation from wet soil surface (E_S) have been modified from *Zhuang et al*. [2002] to calculate E_S on a daily time step rather than a monthly time step.

D4. Snow Sublimation from Ground (S_S)

Daily snow sublimation from the ground (S_S) has been updated from *Zhuang et al*. [2002] by modifying the dynamics of snowmelt. The snowmelt rate (S_{melt}) now uses a daily time step, which depends on daily air temperature and solar radiation [Edward Rastetter, Personal Communication, 2002, *Brubaker et al*., 1996]:

$$S_{melt} = mq \times (\frac{R_n / 100.0}{0.2388}) + A_R \times A_T \quad \text{(Eq. D4)}$$

where *mq* is a constant (2.99 kg MJ^{-1}), R_n is the incident solar radiation to the ground snow, A_R is a constant (2.0 mm $^oC^{-1}$ day^{-1}), and A_T is the daily air temperature.

D5. Upland Soils

In *Zhuang et al.* [2002], the soil profile has been represented with three soil layers: a moss or litter layer, an organic soil layer, and a mineral soil layer. Overall, changes to the water content of the whole soil profile (S) depends on infiltration (I_F), evapotranspiration from the vegetation canopy (E_V), evaporation from the soil surface (E_S), and drainage from the deep mineral layer:

$$\frac{dS}{dt} = I_F - E_V - E_S - D_R \quad \text{(Eq. D5.1)}$$

Within each soil layer, changes in water content are determined using a water balance approach similar to that described in equation D5.1. The terms I_F and D_R are replaced by percolation into and out of a soil layer, respectively, and E_S and S_S are assumed to occur only from the top moss or litter layer. Soil moistures are assumed to be uniformly distributed within each of the three soil layers.

To improve our simulation of water dynamics in upland soils in high latitude ecosystems, we now represent the soil profile with six layers with different hydrologic characteristics: a 10 cm thick moss or litter layer, a 20 cm thick upper organic soil layer, a 40 cm thick lower organic soil layer, a 80 cm thick upper mineral soil layer, a 160 cm thick lower mineral soil layer, and a 320 cm thick deep mineral soil layer. Changes to the water content of the entire soil profile are still influenced by the factors given in Equation D5.1, but soil moisture between the six layers are now assumed to obey the Q-based Richards equation [*Hillel*, 1980; *Celia et al*., 1990]:

$$\frac{\partial W_C}{\partial t} = \frac{\partial}{\partial z}(k(\frac{\partial W_C}{\partial z}\frac{\partial \psi_S}{\partial W_C} + 1)) \quad \text{(Eq. D5.2)}$$

where W_C is the volumetric water content, k is the hydraulic conductivity, and (ψ_s) is the soil matrix potential, which varies as a function of W_C and soil texture [*Clapp and Hornberger*, 1978]. To solve the above equation, the upper boundary condition is set by the infiltration (I_F) from the first soil layer. The lower boundary condition is set to the drainage (D_R) of the deep

mineral soil layer, which is equal to the water conductivity of this layer. The numerical solution of soil water content (W_C) for the middle of each of the different layers of the unsaturated soils is obtained through solving tridiagonal systems with Eq. D5.1 and Eq. D5.2 [see *Press et al*., 1990]. To estimate the soil moisture at each 1 cm depth, the soil moisture contents are interpolated across the six soil layers.

D6. Wetland Soils

Because *Zhuang et al.* [2002] only considered water dynamics in unsaturated soils, new algorithms needed to be developed to estimate the proportion of the soil profile that becomes saturated, the depth of the resulting water table, and the influence of the water table on soil moisture in the unsaturated portion of the soil profile. We assume that wetland soils are always saturated below 30 cm, which represents the maximum water table depth (Z_b). Thus, changes in water content (S) of the top 30 cm of the soil profile can be calculated with a water balance model that considers the water input and outputs at the daily time step:

$$\frac{dS}{dt} = I_F - E_V - E_S - Q_{DR} \qquad \text{(Eq. D6.1)}$$

where I_F is infiltration, E_V is evapotranspiration of the vegetation canopy, E_S is evaporation from the soil surface, and Q_{DR} is the saturated flow drainage below Z_b. Calculation of the I_F, E_T, and E_V terms have been described in the previous sections of Appendix D. Similar to *Walter et al*., [2001a], Q_{DR} is calculated as:

$$Q_{DR} = Q_{DRMAX} \times (Sand \times PV_{SAND} + Silt \times PV_{SILT} + Clay \times PV_{CLAY}) \times 0.01 \qquad \text{(Eq. D6.2)}$$

where Q_{DRMAX} is the maximum drainage rate of 20 mmday^{-1}; PV_{SAND}, PV_{SILT}, and PV_{CLAY} are the constants 0.45, 0.20, and 0.14, respectively and sand, silt, and clay are the proportion of different size fractions in the soil.

Instead of the six layers used to simulate upland soils, we assume that water dynamics in wetland soils can be represented by two functional horizons: an upper oxygenated, unsaturated layer; and a lower anoxic, saturated layer. The water table represents the boundary between these two horizons and it's depth is allowed to change over time with changes in soil moisture. The maximum thickness of the upper unsaturated layer is represented by the maximum water table depth (Z_b), which is assumed to be 30 cm [*Frolking*, 1996; *Granberg et al*., 1999]. The minimum thickness of the lower saturated layer is the difference between the depth of the lower boundary (L_B) and 30 cm. The total volume of water in the top 30 cm of the soil profile (V_{TOT}) is represented by:

$$V_{TOT} = \phi(z_b - W_T) + \int_0^{W_T} \theta_{us}(z)dz \qquad \text{(Eq. D6.3)}$$

where ϕ is the soil porosity, Z_b is the maximum water table depth, W_T is the actual water table depth, and $\theta_{us}(z)$ is the volumetric water content in the unsaturated zone at depth z. We assume ϕ is equal to 0.9 $cm^3\ cm^{-3}$ *[Frolking*, 1996] for the entire soil profile. If S is greater than $Z_b \times \phi$, the water table will be above the soil surface and the height of water above the soil surface is determined by the difference of S and $Z_b \times \phi$. Otherwise, V_{TOT} is equal to S and we can then invert Eq. D.6.3, to solve for the water table depth (W_T) following *Granberg et al*. [1999]:

$$W_T = \sqrt{\frac{3(\phi \times z_b - S)}{2a_z}} \quad \text{if } z \le z_{\theta s,\min} \qquad \text{(Eq. D6.4a)}$$

$$W_T = \frac{3(\phi \times z_b - S)}{2(\phi - \theta_{s,\min})} \quad \text{if } z > z_{\theta s,\min} \qquad \text{(Eq. D6.4b)}$$

where a_z is a constant (6.5, based on a soil porosity of 0.9 $cm^3\ cm^{-3}$), $\theta_{s,min}$ is the minimum volumetric water content of the soil surface and $Z_{\theta s,min}$ is the maximum depth where evaporation influences soil moisture. We assume $\theta_{s,min}$ is 0.25 and $Z_{\theta s,min}$ is 10 cm for all wetland soils. A negative value of the water table depth indicates the water table is above the soil surface whereas a positive value indicates the water table is below the soil surface.

After determining the water table depth, the volumetric water content at each 1 cm depth can then be estimated. If depth z is in the saturated zone, the volumetric water content is assumed to be equal to ϕ. If depth z is in the unsaturated zone, the volumetric water content (θ_{us}) is estimated following *Granberg et al*. [1999]:

$$\theta_{us} = \min(\phi, \theta_s + (\phi - \theta_s)(\frac{z}{W_T})^2) \qquad \text{(Eq. D6.5)}$$

where θ_s is the volumetric water content at the soil surface and is calculated as:

$$\theta_s = \max(\theta_{s,\min}, \phi - (a_z \times W_T)) \qquad \text{(Eq. D6.6)}$$

REPORT SERIES of the MIT *Joint Program on the Science and Policy of Global Change*

1. **Uncertainty in Climate Change Policy Analysis** *Jacoby & Prinn* December 1994
2. **Description and Validation of the MIT Version of the GISS 2D Model** *Sokolov & Stone* June 1995
3. **Responses of Primary Production & C Storage to Changes in Climate and Atm. CO_2 Concentration** *Xiao et al.* Oct 1995
4. **Application of the Probabilistic Collocation Method for an Uncertainty Analysis** *Webster et al.* January 1996
5. **World Energy Consumption and CO_2 Emissions: 1950-2050** *Schmalensee et al.* April 1996
6. **The MIT Emission Prediction and Policy Analysis (EPPA) Model** *Yang et al.* May 1996
7. **Integrated Global System Model for Climate Policy Analysis** *Prinn et al.* June 1996 (*superseded by No. 36*)
8. **Relative Roles of Changes in CO_2 & Climate to Equilibrium Responses of NPP & Carbon Storage** *Xiao et al.* June 1996
9. **CO_2 Emissions Limits: *Economic Adjustments and the Distribution of Burdens*** *Jacoby et al.* July 1997
10. **Modeling the Emissions of N_2O & CH_4 from the Terrestrial Biosphere to the Atmosphere** *Liu* August 1996
11. **Global Warming Projections: *Sensitivity to Deep Ocean Mixing*** *Sokolov & Stone* September 1996
12. **Net Primary Production of Ecosystems in China and its Equilibrium Responses to Climate Changes** *Xiao et al.* Nov 1996
13. **Greenhouse Policy Architectures and Institutions** *Schmalensee* November 1996
14. **What Does Stabilizing Greenhouse Gas Concentrations Mean?** *Jacoby et al.* November 1996
15. **Economic Assessment of CO_2 Capture and Disposal** *Eckaus et al.* December 1996
16. **What Drives Deforestation in the Brazilian Amazon?** *Pfaff* December 1996
17. **A Flexible Climate Model For Use In Integrated Assessments** *Sokolov & Stone* March 1997
18. **Transient Climate Change & Potential Croplands of the World in the 21st Century** *Xiao et al.* May 1997
19. **Joint Implementation: *Lessons from Title IV's Voluntary Compliance Programs*** *Atkeson* June 1997
20. **Parameterization of Urban Sub-grid Scale Processes in Global Atmospheric Chemistry Models** *Calbo et al.* July 1997
21. **Needed: A Realistic Strategy for Global Warming** *Jacoby, Prinn & Schmalensee* August 1997
22. **Same Science, Differing Policies; *The Saga of Global Climate Change*** *Skolnikoff* August 1997
23. **Uncertainty in the Oceanic Heat and Carbon Uptake & their Impact on Climate Projections** *Sokolov et al.* Sept 1997
24. **A Global Interactive Chemistry and Climate Model** *Wang, Prinn & Sokolov* September 1997
25. **Interactions Among Emissions, Atmospheric Chemistry and Climate Change** *Wang & Prinn* September 1997
26. **Necessary Conditions for Stabilization Agreements** *Yang & Jacoby* October 1997
27. **Annex I Differentiation Proposals: *Implications for Welfare, Equity and Policy*** *Reiner & Jacoby* October 1997
28. **Transient Climate Change & Net Ecosystem Production of the Terrestrial Biosphere** *Xiao et al.* November 1997
29. **Analysis of CO_2 Emissions from Fossil Fuel in Korea: 1961–1994** *Choi* November 1997
30. **Uncertainty in Future Carbon Emissions: *A Preliminary Exploration*** *Webster* November 1997
31. **Beyond Emissions Paths: *Rethinking the Climate Impacts of Emissions Protocols*** *Webster & Reiner* November 1997
32. **Kyoto's Unfinished Business** *Jacoby, Prinn & Schmalensee* June 1998
33. **Economic Development and the Structure of the Demand for Commercial Energy** *Judson et al.* April 1998
34. **Combined Effects of Anthropogenic Emissions & Resultant Climatic Changes on Atmosph. OH** *Wang & Prinn* April 1998
35. **Impact of Emissions, Chemistry, and Climate on Atmospheric Carbon Monoxide** *Wang & Prinn* April 1998
36. **Integrated Global System Model for Climate Policy Assessment: *Feedbacks and Sensitivity Studies*** *Prinn et al.* June 1998
37. **Quantifying the Uncertainty in Climate Predictions** *Webster & Sokolov* July 1998
38. **Sequential Climate Decisions Under Uncertainty: *An Integrated Framework*** *Valverde et al.* September 1998
39. **Uncertainty in Atmospheric CO_2 (Ocean Carbon Cycle Model Analysis)** *Holian* October 1998 (*superseded by No. 80*)
40. **Analysis of Post-Kyoto CO_2 Emissions Trading Using Marginal Abatement Curves** *Ellerman & Decaux* October 1998
41. **The Effects on Developing Countries of the Kyoto Protocol & CO_2 Emissions Trading** *Ellerman et al.* November 1998
42. **Obstacles to Global CO_2 Trading: *A Familiar Problem*** *Ellerman* November 1998
43. **The Uses and Misuses of Technology Development as a Component of Climate Policy** *Jacoby* November 1998
44. **Primary Aluminum Production: *Climate Policy, Emissions and Costs*** *Harnisch et al.* December 1998
45. **Multi-Gas Assessment of the Kyoto Protocol** *Reilly et al.* January 1999
46. **From Science to Policy: *The Science-Related Politics of Climate Change Policy in the U.S.*** *Skolnikoff* January 1999
47. **Constraining Uncertainties in Climate Models Using Climate Change Detection Techniques** *Forest et al.* April 1999
48. **Adjusting to Policy Expectations in Climate Change Modeling** *Shackley et al.* May 1999
49. **Toward a Useful Architecture for Climate Change Negotiations** *Jacoby et al.* May 1999
50. **A Study of the Effects of Natural Fertility, Weather & Productive Inputs in Chinese Agriculture** *Eckaus & Tso* July 1999
51. **Japanese Nuclear Power and the Kyoto Agreement** *Babiker, Reilly & Ellerman* August 1999
52. **Interactive Chemistry and Climate Models in Global Change Studies** *Wang & Prinn* September 1999
53. **Developing Country Effects of Kyoto-Type Emissions Restrictions** *Babiker & Jacoby* October 1999
54. **Model Estimates of the Mass Balance of the Greenland and Antarctic Ice Sheets** *Bugnion* October 1999
55. **Changes in Sea-Level Associated with Modifications of Ice Sheets over 21st Century** *Bugnion* October 1999
56. **The Kyoto Protocol and Developing Countries** *Babiker, Reilly & Jacoby* October 1999
57. **Can EPA Regulate GHGs Before the Senate Ratifies the Kyoto Protocol?** *Bugnion & Reiner* November 1999
58. **Multiple Gas Control Under the Kyoto Agreement** *Reilly, Mayer & Harnisch* March 2000

Contact the Joint Program Office to request a copy. The Report Series is distributed at no charge.

Contact the Joint Program Office to request a copy. The Report Series is distributed at no charge.